ASM | mSystems

| Human Microbiome | Research Article

Differential metabolite production underlies disruption of the cystic fibrosis airway microbiota by pathogens

Sydney M. Morabbi,[1] Niladri Bhowmik,[1] Shaz Sutherland,[2] Evelyn A. Wylie,[1] Reagan S. Decker,[1] Akram Al Daerwish,[1] Mercedes Pérez Pérez,[1] Elizabeth Pascual,[1] Erika I. Lutter,[1] Benjamin Philmus,[2] Reed M. Stubbendieck[1]

AUTHOR AFFILIATIONS See affiliation list on p. 26.

ABSTRACT Cystic fibrosis (CF) results in accumulation of mucus in the airways that promotes pathogen colonization, leading to respiratory exacerbations, lung failure, and death. The CF airway harbors a complex microbiota, including pathogens and oropharyngeal bacteria. Here, we reanalyzed 5,260 16S rRNA gene microbiota data sets to infer associations between members of the CF microbiota. We determined that pathogens are more likely to proliferate and dominate when present, while oropharyngeal bacteria are generally present at lower abundances. We found that higher diversity and increasing numbers of pairwise associations between bacteria were positively correlated with lung function. In contrast, dominance of the microbiota by pathogens was associated with loss of lung function. We determined that pathogens are largely negatively associated with each other and oropharyngeal bacteria, suggesting they are antagonistic toward other bacteria. As a first test of this hypothesis, we cultured 1,597 isolates from 96 people with CF and performed 12,542 coculture assays against eight representative pathogens and oropharyngeal bacteria, finding 23% of interactions resulted in inhibition. Among our isolates, *Pseudomonas* were the most inhibitory, but we observed variable activity between different isolates. We further found *Pseudomonas aeruginosa* isolates, even those from the same donor and time point, exhibited significant differences in their metabolome and bioactivity profiles that correlated with acquisition of mutations. Together, our results suggest that pathogens may disrupt the CF microbiota and proliferate in part through bioactive metabolite production. Furthermore, these data highlight that characterizing multiple isolates is necessary to capture the full landscape of chemically mediated interactions within microbiomes.

IMPORTANCE The cystic fibrosis (CF) airway harbors a complex microbiota, including oropharyngeal bacteria and opportunistic pathogens that establish chronic infections. We found that microbiota diversity is correlated with health and that a pathogen-dominated microbiota is associated with low lung function. We then inferred potential microbial interactions by determining abundance associations between CF genera, which suggested that pathogens antagonize other bacteria. To test this prediction, we cultured bacteria from people with CF and performed thousands of coculture assays, finding that approximately one-quarter of interactions resulted in growth inhibition. *Pseudomonas* broadly inhibited other members of the CF airway microbiota. However, we observed marked variability in bioactivity and metabolite profiles of *Pseudomonas aeruginosa* isolates, even from the same donor at the same time. Our results suggest that pathogens disrupt the CF microbiota, possibly through bioactive metabolite production, and that characterizing multiple isolates is necessary to capture the complete picture of interactions in these communities.

KEYWORDS antagonism, cystic fibrosis, lung microbiome, microbial ecology, microbial interactions, natural products, *Pseudomonas aeruginosa*, secondary metabolites

Editor Julia Willett, University of Minnesota Twin Cities, Minneapolis, Minnesota, USA

Address correspondence to Reed M. Stubbendieck, stubbendieck@okstate.edu.

The authors declare no conflict of interest.

See the funding table on p. 27.

Received 3 September 2026
Accepted 11 October 2026
Published 6 November 2026

Copyright © 2026 Morabbi et al. This is an open-access article distributed under the terms of the Creative Commons Attribution 4.0 International license.

Downloaded from https://journals.asm.org/journal/msystems on 06 November 2026 by 139.78.244.80.

Downloaded from https://journals.asm.org/journal/msystems on 06 November 2026 by 139.78.244.80.

Cystic fibrosis (CF) is a genetic disease in humans that results from recessive mutations in the gene encoding the CF transmembrane conductance regulator. As a consequence of these mutations, chloride ion transport is impaired in the respiratory epithelium leading to the accumulation of a thick and dehydrated mucus layer in the lower airways (1, 2), which serves as the substrate for microbial growth (3).

The most well-known bacterial pathogen that colonizes the airways of people with CF (pwCF) is *Pseudomonas aeruginosa*. A long-standing assumption in the field was that *P. aeruginosa* is the sole dominant pathogen in the CF airway. However, a recent meta-analysis revealed that less than half of sputum samples from 507 adults with CF (42.7%) are dominated by this pathogen (relative abundance >50%) (4). In addition to being colonized by other pathogens, such as *Burkholderia cenocepacia* and *Staphylococcus aureus* (5), recent advances in metagenomics and culturomics have confirmed that the airways in pwCF are colonized by a heterogeneous microbiota. This community can include other opportunistic pathogens (e.g., *Achromobacter*, *Burkholderia*, *Haemophilus*, *Pseudomonas*, and *Staphylococcus*) and oropharyngeal bacteria (e.g., *Neisseria*, *Prevotella*, *Rothia*, *Streptococcus*, and *Veillonella*) (6–8). Together, these 10 highlighted genera were previously reported to represent >85% of reads identified by 16S rRNA gene amplicon sequencing of CF sputum (9, 10).

The specific contribution of microbial interactions toward disease in pwCF remains poorly understood (11, 12). Recent microbiome-wide association studies suggest that bacterial interactions are strong predictors of reduced lung function in pwCF (13). For instance, coculture between CF pathogens can enhance virulence factor production or antibiotic resistance by one or both organisms (14). Furthermore, anaerobic oropharyngeal bacteria can ferment mucins and supply *P. aeruginosa* with short-chain fatty acids as a carbon source (15), and disrupting these mucin fermenters predisposes *P. aeruginosa* to treatment with antibiotics that it normally resists (16, 17). Yet other studies have reported that oral anaerobes are negatively correlated with CF pathogens (8, 18). Adding further complexity, elimination of specific pathogens in the CF airway may open niches for colonization by other opportunistic pathogens, which are normally suppressed by their competitors (10, 19). Thus, determining how antagonistic interactions structure the airway microbiota may be key to predicting disease trajectories and therapeutic outcomes in pwCF.

Previous studies that investigated antagonism between CF bacteria have focused primarily on *P. aeruginosa* cocultured with *S. aureus* (20–22) and *Streptococcus* spp. (23). To date, there have been few large-scale interaction screens to identify antagonism between other members of the CF airway microbiota. For instance, Menetrey et al. recently performed 170 coculture interaction assays between CF and environmental isolates of *P. aeruginosa*, *S. aureus*, *Achromobacter xylosoxidans*, and *Stenotrophomonas maltophilia* and documented 30 instances of growth inhibition, suggesting that antagonistic interactions occur among the CF airway microbiota (24). While their work was more exhaustive than prior studies, many members of the CF airway microbiota have not been tested in coculture with other microbes. Thus, there is a gap in our knowledge regarding antagonism that may occur between members of the CF airway microbiota, including interactions that could be exploited for human benefit.

One major mechanism by which bacteria mediate antagonism is through the production of bioactive secondary metabolites (25, 26). Previous genomic surveys that we performed indicated that biosynthetic gene clusters (BGCs) for secondary metabolite production are common in pathogens and oropharyngeal bacteria that reside within the airways of pwCF (27). Production of these compounds has been demonstrated from several CF pathogens, and these compounds function in a broad range of biological activities, including as antibiotics, siderophores, and virulence factors. For instance, *P. aeruginosa* produces a suite of secondary metabolites, including redox-active phenazines, such as pyocyanin, which contribute to host tissue damage and virulence (28–30), electron transport (31, 32), and microbial interactions (33–35). In addition, this pathogen also produces the iron-binding siderophores pyochelin and pyoverdine (36)

and antibiotics, including the copper-containing fluopsin C (37) and 2-heptyl-4-hydroxyquinoline *N*-oxide (20, 38). However, given that *P. aeruginosa* populations diversify during chronic infection (39) and that secondary metabolite production often varies between strains (40–42), antagonistic phenotypes are unlikely to be uniform even within a single pwCF. This variability suggests that surveys that incorporate multiple isolates from the same pwCF and across multiple pwCF are needed to understand how bioactive metabolites mediate interactions broadly between members of the CF microbiota.

We combined a large-scale reanalysis of microbiota data, culture-based interaction assays, and metabolomics and genomics of select isolates to address the following questions. (i) How does variation in colonization of the CF airway by pathogenic and oropharyngeal bacteria correlate with lung disease? (ii) Do CF bacterial isolates exhibit antagonism toward other CF bacteria? (iii) Does isolate-level variation in inhibitory activity of a CF pathogen correspond to changes in chemistry and genotype? We found that pathogens and oropharyngeal bacteria exhibit differential colonization dynamics in the airways of pwCF. Furthermore, we determined that lung function correlated positively with microbiota diversity and with the number of inferred abundance associations between bacterial genera. Among these potential associations, we ascertained that pathogenic genera exhibited mixed associations with other pathogens but were negatively correlated with oral bacterial genera, all of which were positively correlated with each other. To test antagonistic interactions directly, we cultured 1,597 bacterial isolates from 96 pwCF and performed 12,542 coculture assays against eight CF-associated bacteria to assess their inhibitory activity. We found that CF isolates of *Pseudomonas*, *Bacillus, Klebsiella*, and *Stenotrophomonas* were the most inhibitory, while *Staphylococcus* and *Streptococcus* showed little inhibitory activity. However, we observed extensive variability in inhibitory activity of *Pseudomonas*, even among isolates from the same donor at the same time point. Subsequently, we generated cell-free supernatants from a subset of these *P. aeruginosa* isolates and demonstrated that they exhibited variable metabolome and bioactivity profiles. We then identified mutations associated with BGCs or secondary metabolism broadly that were unique to a *P. aeruginosa* isolate that was less inhibitory in coculture. Together, these data suggest that microbial interactions contribute toward shaping the composition of the airway microbiota in pwCF and that isolate-level variability in bioactive metabolite production is potentially an underappreciated factor underlying these interactions.

RESULTS

Pathogens dominate while oropharyngeal bacteria reach low relative abundances in the CF airway

We were initially interested in determining the effect of microbiota composition on lung function in pwCF. We reanalyzed 5,260 16S rRNA gene amplicon sequencing samples from 49 sequencing studies deposited in the Sequence Read Archive (SRA) (Table S1) using the same pipeline (see Materials and Methods for full details) and identified the composition of each microbiota. We limited our analysis to the genus level, as the amplicon sequencing data we analyzed used different regions of the 16S rRNA gene. Furthermore, this marker possesses variable and low phylogenetic resolution below the genus level (43, 44). This approach enabled us to consolidate all of the data into a single analysis, at the cost of losing lower-level taxonomic resolution (i.e., amplicon sequence variants or operational taxonomic units). While this is a reasonable trade-off, we are unable to differentiate between different *Achromobacter*, *Burkholderia*, *Staphylococcus*, and other genera where multiple species colonize the CF airway (45). Overall, there were 19 genera present at ≥1% relative abundance in the metacommunity of the airways of pwCF (Table 1). For all subsequent analyses, we consider *Achromobacter*, *Burkholderia*, *Escherichia*, *Haemophilus*, *Pseudomonas*, *Staphylococcus*, and *Stenotrophomonas* as "pathogen" genera and the remaining 12 genera as "oropharyngeal" genera. It is important to note that our classification is a simplification, as some of these genera (e.g., *Staphylococcus* and *Streptococcus*) contain members that are pathogens (e.g., *S. aureus*

Downloaded from https://journals.asm.org/journal/msystems on 06 November 2026 by 139.78.244.80.

TABLE 1 Composition of the bacterial metacommunity of the CF airway[a]

Genus	Overall relative abundance (%)	Mean relative abundance (%)	Median relative abundance (%) (IQR)[b]
Streptococcus	23.2	22.2	15.1 (4.5–32.1)
Pseudomonas	**11.4**	**20.0**	**1.7 (0.1–31.3)**
Staphylococcus	**10.9**	**12.5**	**0.3 (0.0–11.2)**
Prevotella	9.0	10.5	5.1 (0.6–15.7)
Haemophilus	**6.0**	**6.8**	**0.7 (0.0–4.6)**
Veillonella	5.8	6.9	3.5 (0.6–10.2)
Rothia	4.9	3.7	0.9 (0.1–4.4)
Stenotrophomonas	**2.9**	**6.0**	**0.0 (0.0–1.1)**
Neisseria	2.9	3.3	0.3 (0.0–2.9)
Granulicatella	2.4	2.6	0.9 (0.2–2.5)
Achromobacter	**2.3**	**6.1**	**0.0 (0.0–0.8)**
Gemella	2.2	2.1	0.6 (0.1–2.6)
Porphyromonas	1.9	3.1	0.4 (0.0–2.5)
Burkholderia	**1.8**	**6.6**	**0.0 (0.0–0.2)**
Fusobacterium	1.2	2.4	0.2 (0.0–1.9)
Actinomyces	1.1	0.8	0.2 (0.0–0.7)
Schaalia	1.1	1.0	0.3 (0.1–1.0)
Alloprevotella	1.0	1.4	0.2 (0.0–1.2)
Escherichia	**1.0**	**3.1**	**0.0 (0.0–0.2)**
Total	93.0		

[a]All bacterial genera at ≥1.0% overall relative abundance from CF airway samples are shown. Pathogen-associated genera are indicated in bold, while oropharyngeal genera are indicated in plain text.
[b]IQR, interquartile range.

Downloaded from https://journals.asm.org/journal/msystems on 06 November 2026 by 139.78.244.80.

and the *Streptococcus anginosus* group) or are benign or beneficial (e.g., *Staphylococcus epidermidis* and the *Streptococcus mitis* group) (46–48). The 16S rRNA gene does not possess sufficient resolution to distinguish between *S. aureus* and *S. epidermidis*. However, most regions of this marker can distinguish between the *S. anginosus* and *S. mitis* groups. In 5,077 out of 5,260 samples with sufficient resolution, we found that 93.6% of the reads from *Streptococcus* spp. were classified as belonging to the *S. mitis* group. Together, these findings, along with the literature, support our grouping of *Staphylococcus* and *Streptococcus* as pathogen and oropharyngeal genera, respectively (45, 49, 50).

The distribution pattern for each genus in the CF airway microbiota is highly skewed, indicating that subsets of the samples account for most of the abundance of each taxon. As one example, the mean relative abundance of *Pseudomonas* is 20.0%, but its median relative abundance is only 1.7% (interquartile range [IQR]: 0.1%–31.3%) (Table 1). This genus is prevalent (defined as ≥1% relative abundance within an individual sample) in 47% of the samples, and it dominates (defined as >50% relative abundance within an individual sample) 15.9% of the samples. *Pseudomonas* exhibits a conditional dominance (defined as dominance/prevalence) of 33.9%, indicating that this genus tends to proliferate to high abundances when it is present (Fig. 1A). Among all genera of CF bacteria, *Pseudomonas* exhibits the highest dominance of any genus. In contrast, the rarer CF pathogenic genera (e.g., *Achromobacter*, *Burkholderia*, and *Stenotrophomonas*) tend to exhibit low prevalence but proportionally high conditional dominance (Fig. 1A). This pattern indicates that when these rarer CF pathogens are present, they tend to dominate the microbiota. The per-genus conditional dominance of pathogens overall (median: 18.4%, IQR: 16.1%–28.7%) is significantly higher compared to that of the oropharyngeal genera (median: 0.6%, IQR: 0.2%–1.4%) (Wilcoxon rank-sum W = 1, P = 6.1e-4) (Fig. 1A). However, when different CF pathogens exhibit dominance in the airways, they generally reach similar relative abundances (median dominant RA: 69.2%–84.0%; Kruskal–Wallis χ^2 = 17.6, df = 6, P = 0.007; all post hoc Benjamini–Hochberg [BH]-adjusted P > 0.05, except for *Burkholderia* and *Stenotrophomonas*

Downloaded from https://journals.asm.org/journal/msystems on 06 November 2026 by 139.78.244.80.

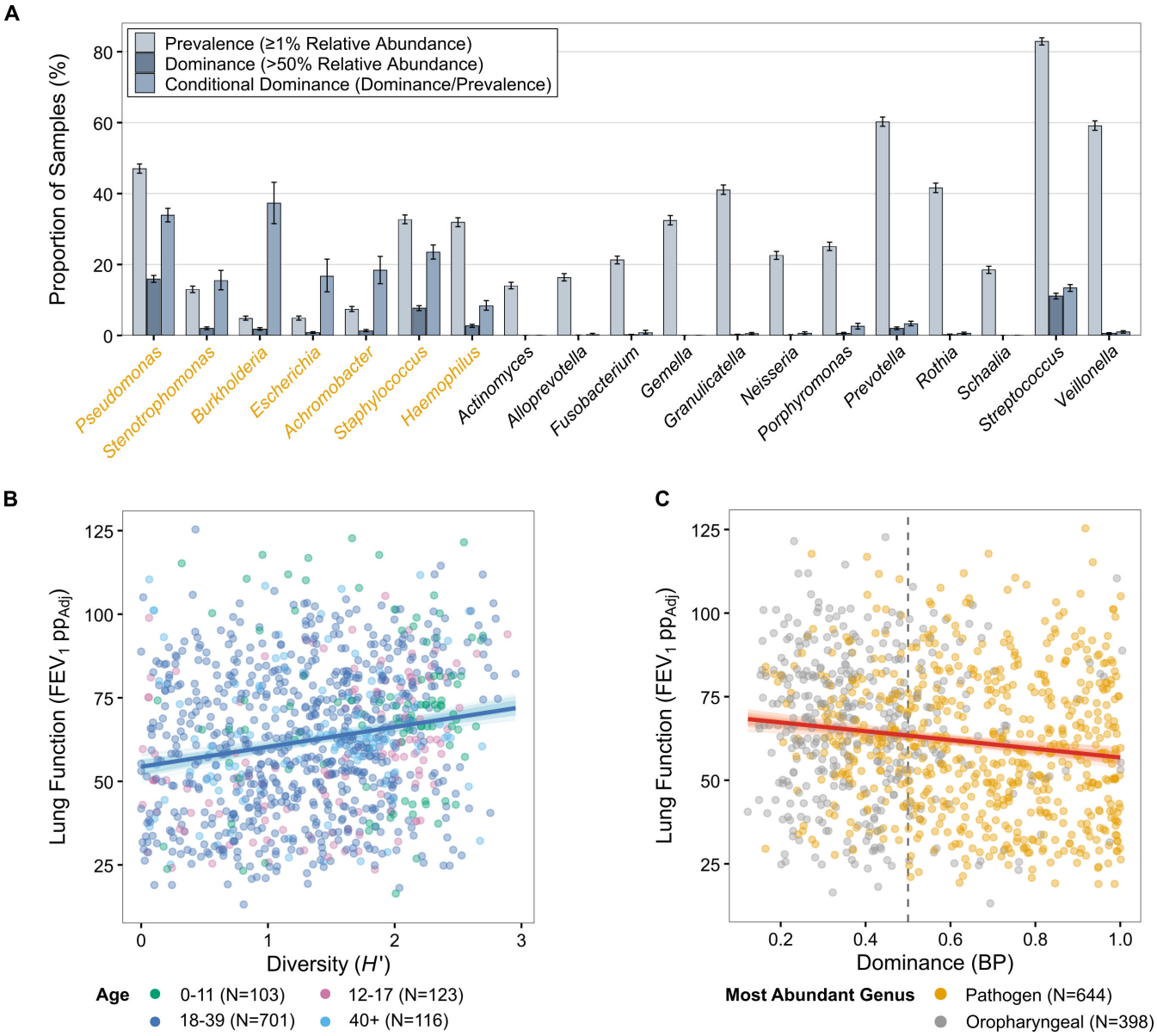


FIG 1 Loss of microbiota diversity and pathogen proliferation are associated with decreased CF lung function. (A) Bar plot showing the prevalence, dominance, and conditional dominance for bacterial genera found in the airways of pwCF. The color of the bar indicates the reported statistic, as indicated in the top left. CF pathogenic genera are indicated in gold. (B) Plot showing the relationship between genus-level Shannon diversity vs lung function based on the forced expiratory volume in 1 s percent predicted after adjustment for BioProject accession number, age, and sample type (FEV_1 pp_{adj}). Each microbiota sample is indicated with a dot, and the color corresponds to the age category indicated below. The blue line indicates the line of best fit, and each of the 100 light blue lines represents a bootstrap replicate of the fit. (C) Plot showing the relationship between the Berger–Parker (BP) dominance and lung function after adjustment for BioProject accession, age, and sample type (FEV_1 pp_{adj}). Each microbiota sample is indicated with a point. Points were jittered to avoid overplotting. Gray and gold points indicate samples where oropharyngeal and pathogens were the most abundant genera, respectively. Points to the right of the dashed line are dominated numerically by a single genus. The red line indicates the line of best fit, and each of the 100 light red lines represents a bootstrap replicate of the fit. See Fig. S5 in the supplemental material for a version of this figure where the points are given different colors for each specific genus of CF pathogen.

vs *Escherichia*) (Fig. S1A). Furthermore, when pathogens dominate a sample, they reach higher relative abundances (median: 78.7%, IQR: 63.8%–92.1%) compared to the oropharyngeal bacteria (median: 67.7%, IQR: 57.0%–83.7%) (Wilcoxon rank-sum W = 528,157, P < 2.2e-16) (Fig. S1B). These patterns are consistent with pathogenic and oropharyngeal genera differing with respect to their colonization dynamics, suggesting that the oropharyngeal genera are typically present at low relative abundance and rarely

dominate the microbiota, whereas the pathogens proliferate to high relative abundance when present.

The overall composition of the CF airway microbiota is only weakly associated with age and lung function, but specific genera are associated with these factors

Given the differences between the dynamics of pathogenic and oropharyngeal genera in the CF airway, we were then interested in determining if other factors influence the composition of this microbiota. For this and all subsequent analyses we pooled all samples together, regardless of repeated sampling from the same individuals longitudinally or replicate sampling from different sites at the same time (see Table S1 in the supplemental material). We performed a permutational multivariate analysis of variance (PERMANOVA) analysis and determined that BioProject accession ($F_{48,5260}$ = 33.61, R^2 = 0.24, BH-adjusted P = 1.2e-4), 16S rRNA gene region sequenced ($F_{7,5260}$ = 35.17, R^2 = 0.045, BH-adjusted P = 1.2e-4), and sample type ($F_{5,5260}$ = 33.1, R^2 = 0.031, BH-adjusted P = 1.2e-4) were the primary contributors to variation in microbiota composition ($F_{53,5260}$ = 17.66, R^2 = 0.15, BH-adjusted P = 1.2e-4) at the genus level, indicating that observed differences were largely driven by technical factors. These technical factors are confounded with the identity of each study and cannot be statistically separated, as each study amplified a single 16S rRNA gene region; 48/49 used the same sequencing platform; 42/49 used a single sample type; and read length was consistent within 40/49 studies. Sequencing depth was the only factor that varied substantially within studies, although depth of samples from within the same study was still more similar than samples from different studies ($F_{48,5211}$ = 199.0, R^2 = 0.65, P < 2.2e-16). Furthermore, effects of DNA extraction and library preparation protocols were likely varied between studies. As such, BioProject accession serves as a composite proxy for technical variation as a whole (see Table S1 in the supplemental material). Subsequently, we performed partial PERMANOVA analyses on subsets of the samples conditioned on these factors and found statistically significant but weak effects of age ($F_{1,2386}$ = 20.39, R^2 = 0.0067, P = 0.001) (Fig. S2A) and lung function, as measured by the forced expiratory volume in 1 s percent predicted (FEV_1 pp) ($F_{1,1103}$ = 17.55, R^2 = 0.0134, P = 0.001) (Fig. S2B), and sex ($F_{1,1618}$ = 12.98, R^2 = 0.0058, P = 0.001) (Fig. S2C) on the microbiota composition. The effects of age and lung function were unchanged when we restricted permutation to within individual studies (i.e., BioProject accessions), persisted when accounting for replication and longitudinal sampling of the same individuals (see Table S2 in the supplemental material), and were consistent across the majority of individual studies (see Table S3 in the supplemental material). However, the effect of sex was not robust after accounting for repeated sampling, either when we restricted the analysis to a single sample per individual ($F_{1,549}$ = 0.96, R^2 = 0.0013, P = 0.43) or when we averaged the microbiota profile of each individual across all corresponding samples ($F_{1,551}$ = 1.41, R^2 = 0.0018, P = 0.17). Furthermore, the effect of sex was not consistent across the 18 studies where it was reported (see Table S3 in the supplemental material).

The composition of the CF airway microbiota has been reported to shift with age. Specifically, it is often reported that *S. aureus* is more likely to colonize younger individuals, while *P. aeruginosa* is more likely to colonize older individuals (51). We compared the odds ratio for colonization by each of the 19 most abundant bacterial genera that colonize the airways of pwCF in adults (≥18 years, N = 724 individuals) and children (<18 years, N = 381 individuals). Consistent with prior reports, we found that the odds for colonization by *Pseudomonas* were significantly higher in adults, whereas the odds for colonization by *Haemophilus* were higher in children. In addition, the odds for colonization by *Granulicatella*, *Gemella*, *Neisseria*, and *Schaalia* were significantly higher in children. There was no difference in the odds for colonization by the other pathogens and oropharyngeal genera between these age groups (see Fig. S3A in the supplemental material). Furthermore, we confirmed that the odds for colonization by the pathogens *Pseudomonas* and *Achromobacter* increased in pwCF with worse lung

Downloaded from https://journals.asm.org/journal/msystems on 06 November 2026 by 139.78.244.80.

function. In contrast, the odds for colonization by the oropharyngeal bacteria, with the exception of *Porphyromonas*, increased in individuals with higher lung function. The pathogen *Haemophilus* was also associated with better lung function (see Fig. S3B in the supplemental material).

Together, these analyses suggest that age and lung function exert weak but reproducible effects on the overall composition of the CF airway microbiota at the genus level. However, *Pseudomonas* is associated with adults and pwCF with worse lung function, while the oropharyngeal bacteria are associated with children and pwCF with better lung function.

Decreased microbiota diversity and increased pathogen dominance are associated with decreased lung function in CF

We next examined if other microbial factors were related to lung function. We determined that the alpha diversity of CF airway samples, as estimated with the Shannon diversity index (*H′*), was positively associated with lung function in pwCF (regression coefficient [*b*]: +6.5 FEV_1 pp per 1 unit *H′*, $t = 6.63$, $P = 5.6e\text{-}11$; full-model adjusted $R^2 = 0.23$, with covariates of age, BioProject accession, 16S rRNA region sequenced, and sample type) (Fig. 1B), consistent with prior reports (7, 52). This association remained significant after accounting for repeated sampling of the same individuals, both when individual identity was modeled as a random effect ($b = +3.4$ FEV_1 pp per 1 unit *H′*, $t = 5.79$, $P = 1.0e\text{-}8$; marginal $R^2 = 0.11$) and when the analysis was restricted to a single sample per individual with repeated sampling ($b = +5.9$ FEV_1 pp per 1 unit *H′*, $t = 3.91$, $P = 1.1e\text{-}4$; adjusted $R^2 = 0.18$). We then wanted to characterize the effect of microbiota dominance on lung function. We determined dominance for each sample using the Berger–Parker (BP) index, which represents the proportion of the microbiota occupied by the most abundant genus. We observed an inverse correlation between dominance and lung function ($b = -1.4$ FEV_1 pp per 0.1-unit increase in BP, $t = -4.9$, $P = 8.9e\text{-}7$; full-model adjusted $R^2 = 0.21$, with covariates of age, BioProject accession, 16S rRNA region sequenced, and sample type) (Fig. 1C), consistent with a prior report (52). Notably, the majority (86%) of CF airway samples with a BP value of ≥0.5, indicating numeric dominance by a single genus, are pathogen dominated (Fig. 1C; Fig. S3). As before, this association remained significant when individual identity was modeled as a random effect ($b = -0.83$ FEV_1 pp per 0.1-unit increase in BP, $P = 1.9\text{-}7$) and when the analysis was restricted to a single sample per individual with repeated sampling ($b = -1.3$ FEV_1 pp per 0.1-unit increase in BP, $P = 0.005$). Together, these data are consistent with the hypothesis that loss of microbiota diversity and proliferation of pathogens contribute to worse disease in the airways of pwCF (52).

Negative covariation involving pathogens and positive covariation among oropharyngeal bacteria correspond to divergent lung function outcomes in CF

We then wanted to explore potential causes of pathogen dominance in the CF airway and their consequences on lung function. We used linear models to evaluate abundance associations between different CF bacterial genera using the full 16S rRNA gene amplicon sequencing data set. We define the covariation coefficient as the magnitude and direction of the slope (positive or negative) in these models. Of 12 significant abundance associations between two pathogenic genera, 7 (58.3%) of the covariation coefficients were positive and 5 (41.7%) of the covariation coefficients were negative. Notably, in 52 significant abundance associations between pathogenic genera and oropharyngeal genera, 15 (28.8%) of the covariation coefficients were positive and 37 (71.2%) of the covariation coefficients were negative. Most of the positive covariation occurred between *Haemophilus* or *Staphylococcus* and oropharyngeal genera (Fig. 2A). In contrast, we found that all 66 significant abundance associations between oropharyngeal genera had positive covariation coefficients (Fig. 2A). We confirmed that all of these associations were robust to sampling when we modeled individual identity as

Downloaded from https://journals.asm.org/journal/msystems on 06 November 2026 by 139.78.244.80.

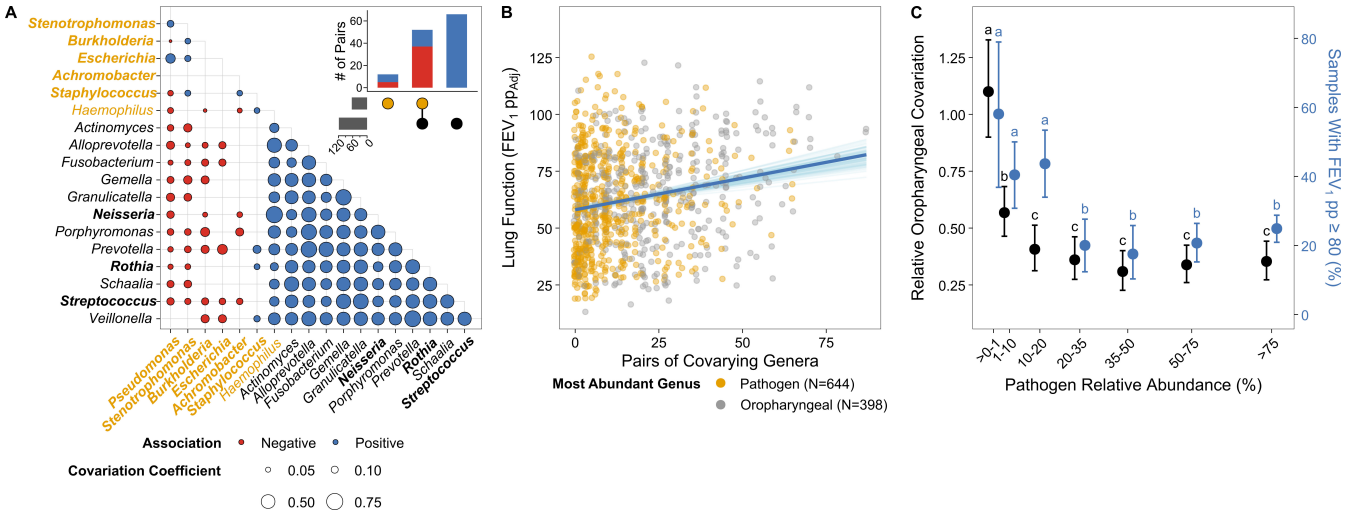


FIG 2 Increasing bacterial covariation is correlated with increased CF lung function. (A) Bubble plot showing associations between bacterial genera in the CF airway based on 5,260 16S rRNA gene amplicon sequencing studies. Genera with CF pathogens are indicated in gold. For genera indicated in bold, there was at least one corresponding CF isolate or target included in coculture assays. Red and blue bubbles indicate negative and positive associations, respectively, and the size of the bubble indicates the strength of the association as measured by the absolute value of the covariation coefficient. For simplicity, only the lower half of the correlation matrix is shown. (Inset) UpSet plot showing the number of significant association pairs by category (top right). The gold and black dots represent pathogens and oropharyngeal bacteria, respectively (bottom left). Bar plot indicating the total number of associations that involve pathogens and oropharyngeal bacteria on the top and bottom, respectively. (B) Plot showing the relationship between the number of covarying genera and lung function after adjustment for age, BioProject accession, 16S rRNA gene region sequenced, and sample type (FEV_1 pp_{adj}). Each microbiota sample is indicated with a point. Gray and gold points indicate samples where oropharyngeal, and pathogens were the most abundant genera, respectively. Points were jittered to avoid overplotting. The blue line indicates the line of best fit, and each of the 100 light blue lines represents a bootstrap replicate of the fit. (C) Plot showing the relationship between pathogen relative abundance and the mean covariation coefficient among the oropharyngeal genera (black points, left axis) and the proportion of samples from pwCF with high lung function (blue points, right axis). The covariation coefficients were calculated as in panel A but with pathogenic genera excluded from the abundance matrix before averaging across all 66 pairs and expressed relative to samples with no pathogens. The points and error bars correspond to the mean and the 95% CI of 2,000 bootstrap draws. Pathogen relative abundance bins sharing a letter are not significantly different and are assigned separately for each series. The covariation was calculated from 3,764 samples, and lung function was assessed using 1,084 samples with a recorded FEV_1 pp value.

a random effect (matched association signs: 97%, concordance correlation coefficient [CCC]: 0.95) and when the analysis was restricted to a single sample per individual with repeated sampling (matched association signs: 97%, CCC: 0.98). To test the sensitivity of this analysis to the 16S rRNA gene region sequenced, we refit the abundance model within each sequenced region and compared the resulting coefficients to those for the pooled analysis. With the exception of the V1–V3 (N = 154) and V3 (N = 20) regions, which were undersampled, there was strong agreement between the individual regions and the pooled analysis (matched signs: 83%–97%, CCC: 0.79–0.93, and Spearman rank: 0.78–0.93) (see Fig. S4 in the supplemental material).

We observed that as the number of predicted covarying genera in a sample increased, lung function was higher (b = +0.31 FEV_1 pp per genus pair, t = 7.1, P = 2.3e-12; full-model adjusted R^2 = 0.23, with covariates of age, BioProject accession, 16S rRNA region sequenced, and sample type) (Fig. 2B). We found that this association was also robust when individual identity was modeled as a random effect (b = +0.13 FEV_1 pp per genus pair, P = 5.4e-7) and when the analysis was restricted to a single sample per individual with repeated sampling (b = +0.31 FEV_1 pp per genus pair, P = 4.9e-6). To place this finding in the context of the microbiota diversity analyses from above, we compared the relative contributions of abundance associations, dominance, and diversity to lung function using separate models conditioned on BioProject accession, age, and sample type. The number of covarying genera had a similar effect (absolute value of the standardized regression coefficient [|b*|] = 4.96 FEV_1 pp/standard deviation [SD], P = 2.3e-12) on microbiota diversity (|b*| = 4.60 FEV_1 pp/SD, P = 5.6e-11), whereas

Downloaded from https://journals.asm.org/journal/msystems on 06 November 2026 by 139.78.244.80.

the effect of dominance was weaker ($|b^*|$ = 3.45 FEV_1 pp/SD, P = 8.9e-7). However, it is important to note here that these factors are interrelated (diversity and dominance are correlated at $r = -0.95$).

The preponderance of negative associations between pathogen and oropharyngeal genera prompted us to investigate the influence of pathogens on community structure. We binned samples based on the relative abundance of pathogens, removed the pathogenic genera from the abundance matrix, rarefied each sample to a common depth, and recalculated their covariation relative to samples with no detected pathogens. We determined that an increase of up to 10%–20% in the relative abundance of pathogens was concomitant with a decrease in covariation between oropharyngeal genera (Fig. 2C). This result suggests that the presence of pathogens may disrupt the positive associations that occur between oropharyngeal genera. Note, because the pathogens are removed from this analysis, this decline in covariation cannot be attributed to the composite effects of pathogen relative abundance. There is also a potential concurrent effect on lung function: as oropharyngeal covariation decreases, the percentage of samples with high lung function (defined as FEV_1 pp ≥80) also decreases (Spearman r_s = 0.86, 95% CI: 0.39–0.96, P = 5e-4) (Fig. 2C). In summary, these microbiota data indicate that abundance associations within the CF airway are linked to lung health. Specifically, these data lead us to hypothesize that while oropharyngeal bacteria exhibit potential cooperative interactions and are thought to be beneficial for CF lung function (18), pathogens potentially exhibit antagonistic interactions, disrupt the microbiota, and impair lung function.

Isolation and identification of bacteria from CF clinical samples

For subsequent *in vitro* experiments, we generated a collection of 1,597 CF bacterial isolates from 96 pwCF. We provide specific details for the donors and bacterial isolates in Table S4 and Table S5, respectively, in the supplemental material. To identify the bacteria, we performed colony PCR and high-throughput sequencing of the 16S rRNA gene V3–V4 region and then classified sequences using the eHOMD (53). Together, the genera *Staphylococcus* (*n* = 630), *Pseudomonas* (*n* = 558), *Bacillus* (*n* = 88), *Enterococcus* (*n* = 78), *Lacticaseibacillus* (*n* = 53), *Klebsiella* (*n* = 38), *Streptococcus* (*n* = 38), *Escherichia* (*n* = 19), *Stenotrophomonas* (*n* = 19), and *Microbacterium* (*n* = 12) represented 96% of the total isolates that we cultured (see Table S5 in the supplemental material). Note that each of these genera was detected in the amplicon sequencing data, though some were below 1% mean relative abundance. Given their abundance in pwCF, high growth rate, and non-fastidious nature, it is not surprising that *Pseudomonas* and *Staphylococcus* were the most common isolates in our collection. The remaining 4% of isolates (*n* = 64) consisted of genera with <10 representative isolates or were unclassified at the genus level. We classified these latter isolates as "other" (see Table S5 in the supplemental material). Together, this collection of isolates contains bacterial genera representing 7 of 19 of the most abundant genera (≥1% relative abundance) in the CF metacommunity and 7 of 14 of the most abundant (≥1% relative abundance) aerobic or facultative anaerobic genera (Table 1).

CF isolates inhibit respiratory bacteria

To test the hypothesis that the negative associations that we inferred from amplicon sequencing studies would replicate in the laboratory, we performed coculture inhibition assays. In total, we tested 1,597 CF isolates for their ability to inhibit a single strain of the following bacteria: *A. xylosoxidans*, *B. cenocepacia*, *Burkholderia cepacia*, *Neisseria meningitidis*, *P. aeruginosa*, *Rothia mucilaginosa*, *S. aureus*, and *Streptococcus oralis* using the cross-streak method. We chose these bacteria as targets because they represented a combination of known pathogens and commensal organisms that commonly colonize the CF airway (8, 10) and were amenable to culturing in our laboratory. We chose *N. meningitidis* as a representative *Neisseria* and as a pathogen of concern and *S. oralis* as a representative *Streptococcus* that grew adequately under our culture conditions. Our

Downloaded from https://journals.asm.org/journal/msystems on 06 November 2026 by 139.78.244.80.

Downloaded from https://journals.asm.org/journal/msystems on 06 November 2026 by 139.78.244.80.

exclusion of a representative *Prevotella* spp., *Veillonella* spp., or other obligate anaerobic bacterial strains was intentional due to the technical challenge of performing coculture assays with a combination of strictly aerobic and anaerobic target organisms.

We performed cross-streak assays to assess the inhibitory activity of each of the CF isolates. After overnight incubation, we measured the zone of inhibition (ZOI) between the isolate and the perpendicular target streaks (Fig. 3A). In total, we measured ZOIs from 12,542 total isolate × target combinations. In the case of 234 of these combinations, there was poor growth of the target on a monoculture control plate, overgrowth of the CF isolate, or contamination. We did not consider these combinations in further analysis. As 44 out of 64 isolates in the other category did not inhibit any of the targets tested, we did not consider any isolates in this category further in this study. We assigned each isolate × target combination a score based on the ZOI of the target: no inhibition (ZOI = 0 cm, score: 0), weak inhibition (ZOI = 0–1.0 cm, score: (1), moderate inhibition (ZOI = 1.0–2.0 cm, score: (2), strong inhibition (ZOI ≥2.0 cm or no observed growth of target, score: (3).

In total, we observed that 2,886 (23% of the total) isolate × target combinations resulted in some level of growth inhibition of the target (i.e., ZOI: >0 cm, score: 1–3) (Fig. 3B). There were significant differences in inhibition of each target (χ^2 = 2,489.9, df = 21; Monte Carlo simulated P < 1.0e-5). We found that *R. mucilaginosa* was the most susceptible to inhibition (50% of interactions resulted in inhibition), followed by *S. oralis* (34%). We observed similar inhibition of *B. cepacia*, *B. cenocepacia*, *N. meningitidis*, and *S. aureus* (21%–28%). As expected, *A. xylosoxidans* (4%) and *P. aeruginosa* (0.3%) were the least inhibited targets (Fig. 3C). In the latter case, there were only four isolates that inhibited *P. aeruginosa*, albeit very weakly (average ZOI = 0.1 cm). We identified one of these inhibitory isolates as a *Microbacterium* and the other three isolates as *Pseudomonas*, which were all derived from the same donor and may represent the same strain.

For each pair of genera that was present in both data sets, we compared the percentage of cross-streak assays in which the target was inhibited to the covariation coefficient we calculated above. The pairs of genera with the highest inhibition frequencies also covaried negatively (e.g., *Pseudomonas* isolates inhibited *R. mucilaginosa* in 79% of assays, covariation coefficient = −0.054), whereas the strongest positively covarying pairs exhibited almost no inhibition (e.g., *Streptococcus* isolates inhibited *R. mucilaginosa* in 11% of assays, covariation coefficient = +0.51; and *Streptococcus* isolates inhibited *N. meningitidis* in 3% of assays, covariation coefficient = +0.27). Across 31 genus pairs, with at least 10 cross-streak assays, we found that *in vitro* inhibition of targets correlated overall with the inferred associations from the 16S rRNA gene microbiota analyses (Spearman r_s = −0.43, P = 0.017) (Fig. 4). These data indicate that the negative associations that we determined from 16S rRNA gene amplicon sequencing data are at least partially recapitulated by antagonistic interactions that occur between the corresponding genera in coculture.

We then sought to determine which CF genera were most inhibitory toward the selected targets by normalizing the inhibition exhibited by each genus by the total number of coculture assay combinations tested. There were significant differences in target inhibition based on isolate genus (χ^2 = 2,612.3, df = 27; Monte Carlo simulated P < 1.0e-5). Consistent with the inferred abundance associations (Fig. 2C), *Pseudomonas* was the most inhibitory genus that we tested (47% of combinations resulted in inhibition) and was approximately 1.5× more inhibitory than the next most inhibitory genus. *Stenotrophomonas*, *Bacillus*, and *Klebsiella* were modestly inhibitory genera (~30%). *Enterococcus* and *Escherichia* were poorly inhibitory genera (~16%). We observed little inhibition by *Microbacterium*, *Lacticaseibacillus*, *Staphylococcus*, and *Streptococcus* (<10%) (Fig. 5A). In the latter case, lack of inhibition by *Staphylococcus* and *Streptococcus* was expected based on the inferred associations (Fig. 2B).

Downloaded from https://journals.asm.org/journal/msystems on 06 November 2026 by 139.78.244.80.

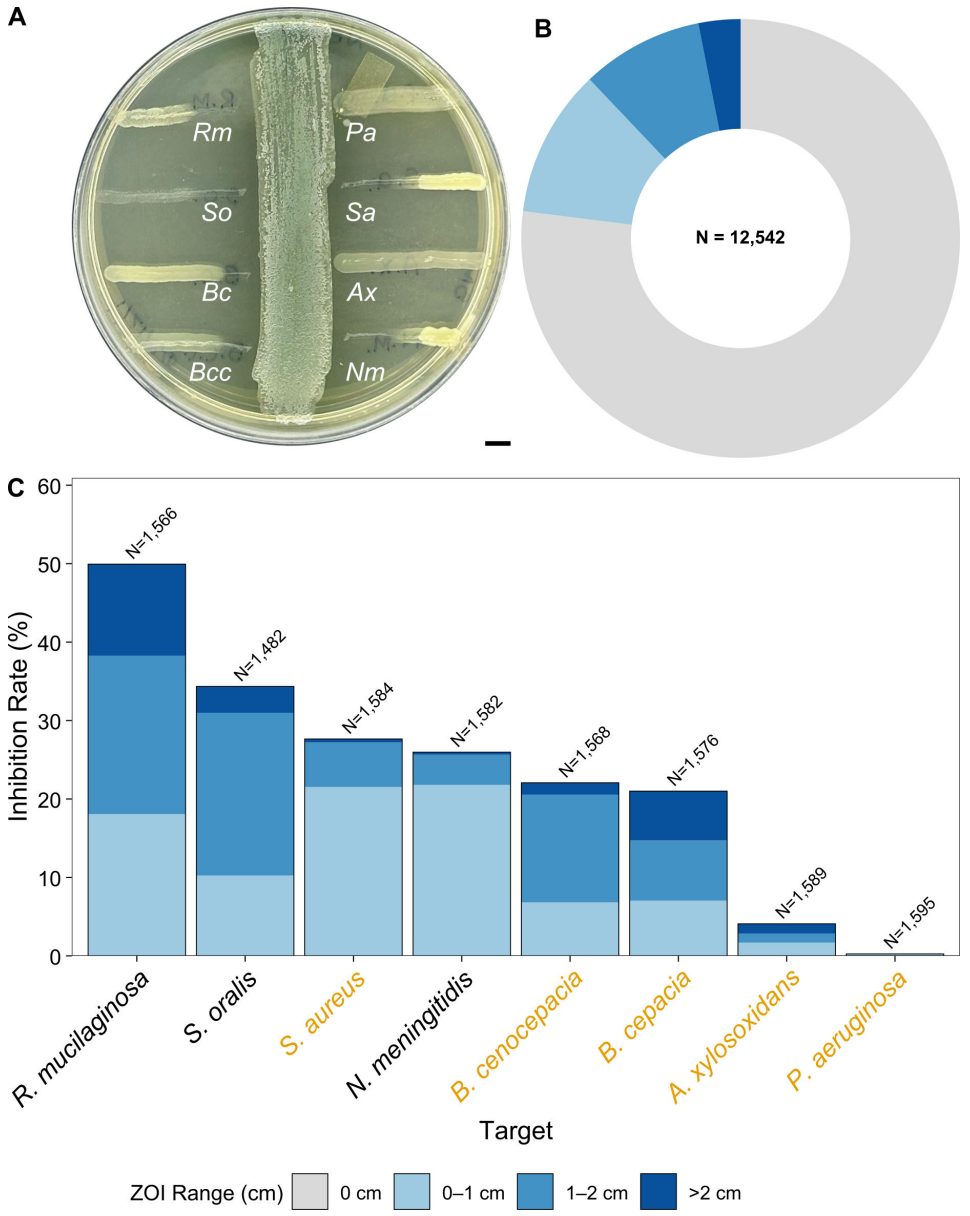


FIG 3 CF isolates inhibit the growth of CF-associated target strains. (A) Photograph of a representative coculture between *Pseudomonas* isolate NB0851 (middle of plate) and eight bacterial target strains. The ZOI is defined as the distance between the CF isolate and the point of growth on the perpendicular target streak. Abbreviations: *Ax*, *A. xylosoxidans* subsp. *xylosoxidans*; *Bc*, *B. cepacia*; *Bcc*, *B. cenocepacia*; *Nm*, *N. meningitidis*; *Pa*, *P. aeruginosa*; *Rm*, *R. mucilaginosa*; *Sa*, *S. aureus*; *So*, *S. oralis* subsp. *oralis*. Scale bar = 5 mm. (B) Donut plot showing the fraction of isolate × target interactions, with each color representing no inhibition (ZOI = 0 cm, score: 0), weak inhibition (ZOI = 0–1.0 cm), moderate inhibition (ZOI = 1.0–2.0 cm), strong inhibition (ZOI ≥2.0 cm or no observed growth of target), as indicated by the legend below. The total number of tested interactions is indicated in the center of the donut. (C) Stacked bar plot showing the frequency of inhibition for each target strain. Each color represents the proportion of interactions that resulted in the corresponding level of inhibition, as indicated by the legend below. The total number of interactions tested involving a given target is specified above each stacked bar. CF pathogens are indicated in gold.

CF isolates possess variable bioactivity against respiratory bacteria

We wanted to identify individual isolates that exhibited strong inhibitory activity. To compare the overall inhibitory activity spectrum of each individual CF isolate, we calculated and compared *Z*-scores based on the total inhibition score across the

Downloaded from https://journals.asm.org/journal/msystems on 06 November 2026 by 139.78.244.80.

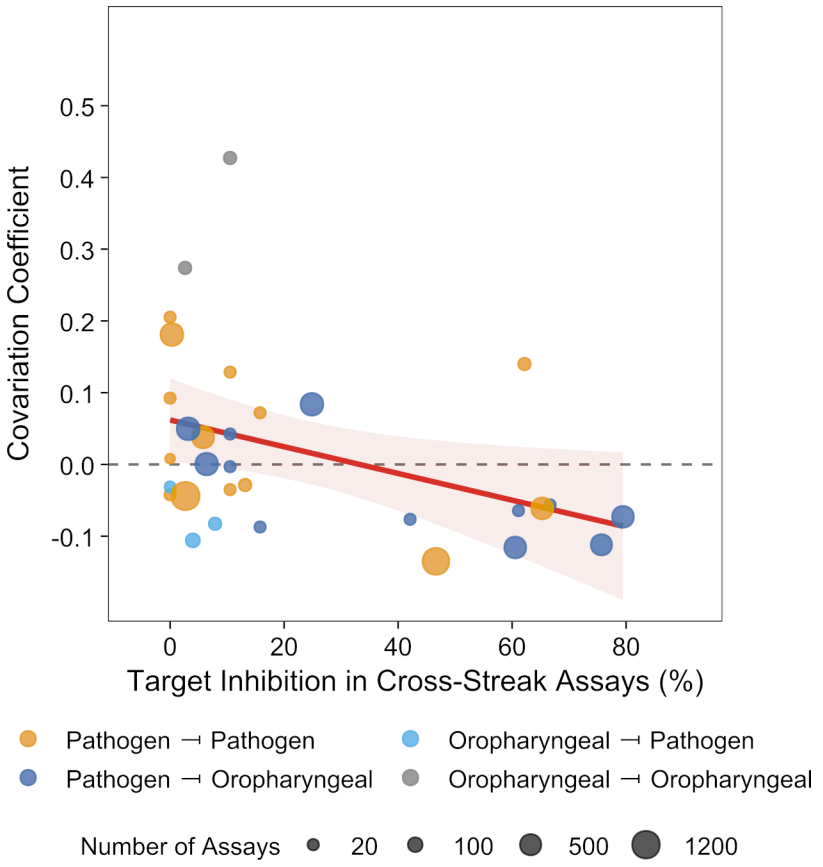


FIG 4 Inhibition *in vitro* corresponds to covariation *in vivo* between members of the CF airway microbiota. The plot shows the relationship between the percentage of cross-streak assays where the target was inhibited (i.e., inhibition score ≥1) and the covariation coefficient from the linear models used to evaluate abundance associations between different CF bacterial genera using the full 16S rRNA gene amplicon sequencing data set. Each point represents one genus-level pair that appears in both the 16S rRNA gene covariation analysis and the cross-streak assays, with either genus serving as the isolate or the target. The color and size of each point correspond to the directionality of the cross-streak assay (i.e., pathogen ⊣ oropharyngeal indicates that a pathogen genus was tested for its inhibitory activity against an oropharyngeal genus) and the number of cross-streak assays involving that pair, respectively. The red line and shading indicate the ordinary least-squares fit and the 95% CI, respectively. For three genus pairs (*Pseudomonas–Staphylococcus*, *Pseudomonas–Streptococcus*, and *Staphylococcus–Streptococcus*), both directions were tested in the cross-streak assays, and only the direction with the higher percentage of inhibited assays is plotted. Pairs with fewer than 10 cross-streak assays were excluded from this analysis.

eight targets. As before, we observed significant differences when comparing the median inhibition *Z*-scores between different genera (Kruskal–Wallis χ^2 = 514.65, df = 9; P < 2.2e-16). (Fig. 5B). Isolates of *Pseudomonas* tended to be the most inhibitory, while isolates of *Staphylococcus* and *Streptococcus* were the least inhibitory. Isolates of *Bacillus*, *Klebsiella*, *Enterococcus*, *Escherichia*, *Microbacterium*, and *Lacticaseibacillus* exhibited intermediate inhibition (Fig. 5B). In addition, across the focal genera, there were significant differences in *Z*-score dispersion, indicating intra-genus variability with respect to inhibitory activity (Fligner–Killeen χ^2 = 527.36, df = 9; P < 2.2e-16). Subsequently, we identified 23 significant differences between the *Z*-score distribution of genera pairs, with *Pseudomonas* exhibiting the most significant differences when compared to the other genera (Fig. 5B).

Downloaded from https://journals.asm.org/journal/msystems on 06 November 2026 by 139.78.244.80.

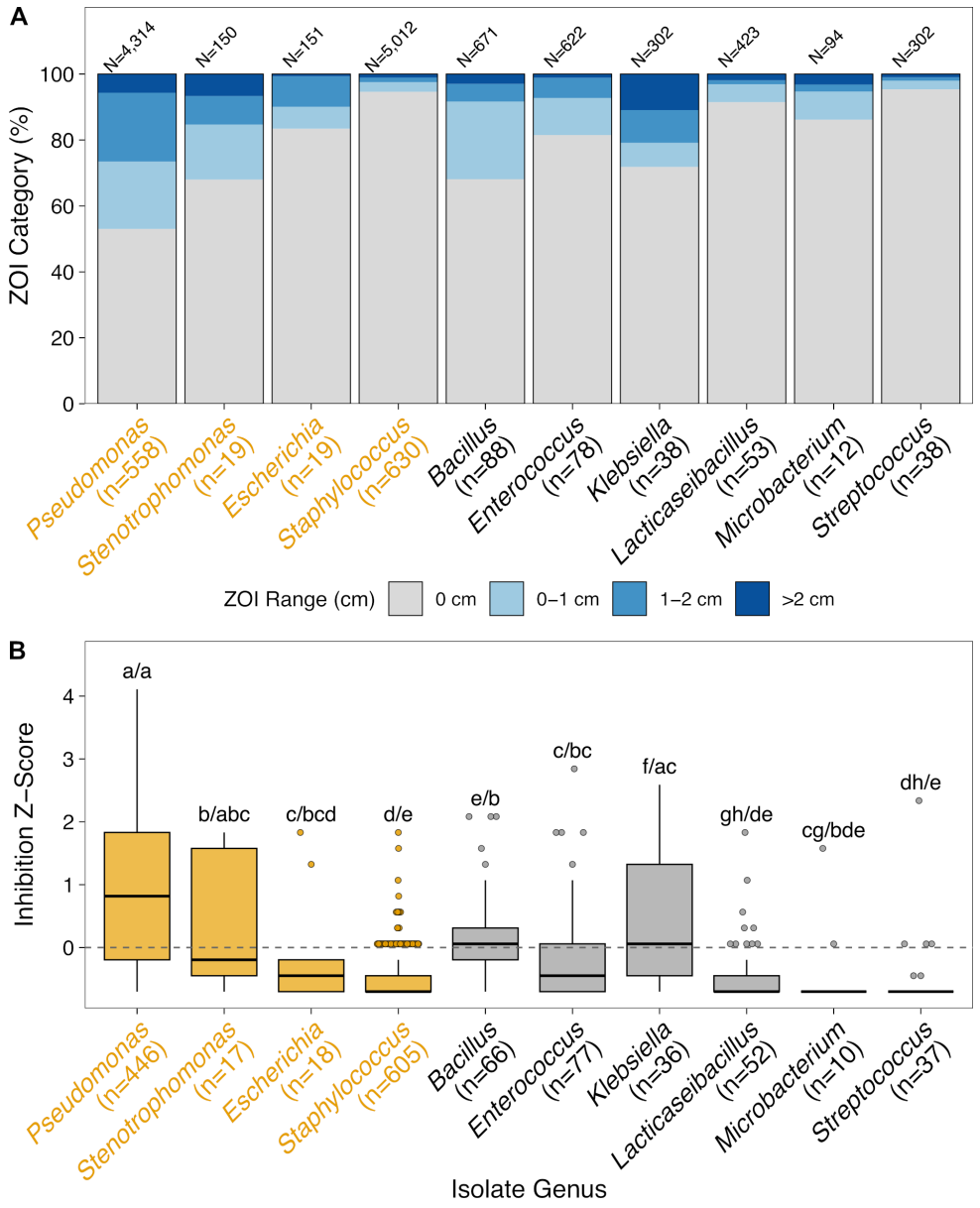


FIG 5 CF isolates exhibit variable inhibition of CF-associated target strains. (A) Stacked bar plot showing the frequency of inhibition exhibited by each genus of CF isolates tested. Each color represents the proportion of interactions that resulted in the corresponding level of inhibition of a target strain, as indicated by the legend below. The total number of isolates tested (*n*) and the total number of interactions assayed (*N*) involving a given CF isolate genus are specified below and above each stacked bar, respectively. (B) Plot showing the *Z*-score normalized inhibition of each CF isolate tested against all target strains. The upper and lower bounds of the box plots indicate the 75th and 25th percentiles, respectively. The horizontal black bars indicate the medians. The whiskers extend from the bounds of the box to the largest and smallest values that are no further than ±1.5× the IQR. Outliers are shown as points. The dashed line indicates the mean inhibition of all isolates (i.e., *Z*-score = 0). The first letter corresponds to the comparisons in *Z*-scores between genera, and the second letter after the slash (/) corresponds to the *Z*-score dispersion between genera. Genera that share letters are not significantly different (BH-adjusted $P > 0.05$). CF pathogens are indicated in gold.

Metabolome profiles vary between *Pseudomonas* isolates from the same donor that exhibit different inhibitory activities

Our coculture inhibition data indicated that *Pseudomonas* is the most antagonistic bacterial genus found in the CF airway. However, there was also significant variability

among inhibitory activity of *Pseudomonas* isolates, with some isolates exhibiting strong inhibition and others that were less inhibitory. (Fig. 5B). Furthermore, we identified 17 cases in which *Pseudomonas* isolates obtained from the same donor at the same time point displayed variable inhibitory activity (within-genus *Z*-score spread: ≥2) (see Fig. 6; Fig. S6 in the supplemental material). These observations suggested the potential of within-host diversification of isolates leading to changes in antagonistic interactions between *Pseudomonas* and other members of the CF microbiota.

We hypothesized that differences in bioactive metabolites produced by these *Pseudomonas* isolates could be responsible for their variable inhibitory activity. As a first test of this hypothesis, we selected two donors (HID07 and HID08) from whom we obtained *Pseudomonas* isolates with varying inhibitory activities in cross-streak assays. We cultured isolates with varying *Z*-scores in triplicate and then assessed the bioactivity of their cell-free supernatants (CFSs) against each of the target bacteria. The CFS of inhibitory *Pseudomonas* isolates (within-genus *Z*-score ≥0) inhibited growth of both *N. meningitidis* and *S. aureus*, while CFSs from the less-inhibitory isolate NB1386 (within-genus *Z*-score: −0.86) had no effect on either target, although it was the only CFS active against *P. aeruginosa* (see Fig. S7A in the supplemental material). In contrast, CFSs from isolate NB1046 (within-genus *Z*-score: −0.43) inhibited *N. meningitidis* and *S. aureus*, which was consistent with the weak inhibitory activity against both targets in coculture.

To determine if there were differences in the composition of CFS from inhibitory and less-inhibitory *Pseudomonas* isolates, we performed untargeted liquid chromatography coupled to tandem mass spectrometry (LC-MS/MS). In total, we aligned 5,645 molecular features (i.e., an *m/z* at a specific retention time), of which 468 varied significantly (multiclass Kruskal–Wallis $P \leq 0.01$) between the six isolates. These molecular features spanned the full chromatographic run and mass range (Fig. 7A). We then wanted to assess whether the metabolome profiles clustered based on the donor or the inhibitory activity. We hierarchically clustered the 468 significant features, which split the CFS from *Pseudomonas* into two well-supported groups (Fig. 7B). We performed marginal PERMANOVA, which indicated that the donor significantly explained variation between *Pseudomonas* isolates ($\omega^2 = 0.31$, $P = 0.011$), whereas the inhibitory phenotype in the coculture had no effect ($\omega^2 = 0.20$, $P = 0.078$) (Fig. S7B). Consistent with this observation, we observed that all CFSs from the HID08 isolates exhibited weak activity against *S. oralis* subsp. *oralis*, while none of the CFSs from HID07 isolates inhibited this target (see Fig. S7A in the supplemental material). Together, these data suggest within-host diversification of *P. aeruginosa* metabolism occurs and that variation in metabolome profiles could be responsible for the differing inhibitory activities of these pathogens.

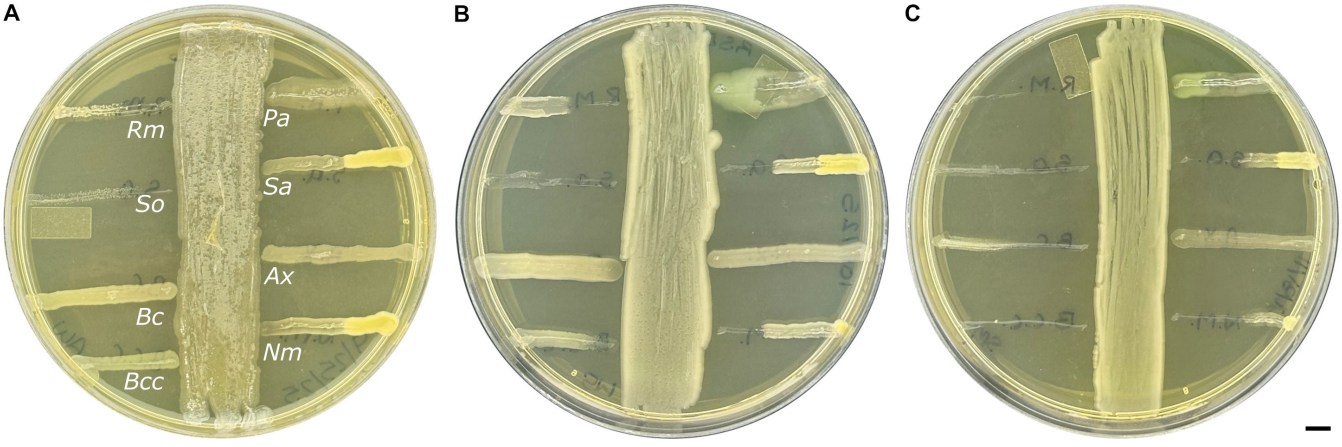


FIG 6 *Pseudomonas* isolates from the same donor and time point exhibit variable inhibition of CF-associated target strains. Photograph of a coculture between *P. aeruginosa* isolate (A) NB1386 (*Z*-score = −0.86), (B) RSD0018 (*Z*-score = 0), and (C) NB0219 (*Z*-score = 1.72) and eight target strains. Scale bar = 5 mm. Abbreviations: *Ax*, *A. xylosoxidans* subsp. *xylosoxidans*; *Bc*, *B. cepacia*; *Bcc*, *B. cenocepacia*; *Nm*, *N. meningitidis*; *Pa*, *P. aeruginosa*; *Rm*, *R. mucilaginosa*; *Sa*, *S. aureus*; *So*, *S. oralis* subsp. *oralis*.

Downloaded from https://journals.asm.org/journal/msystems on 06 November 2026 by 139.78.244.80.

Downloaded from https://journals.asm.org/journal/msystems on 06 November 2026 by 139.78.244.80.

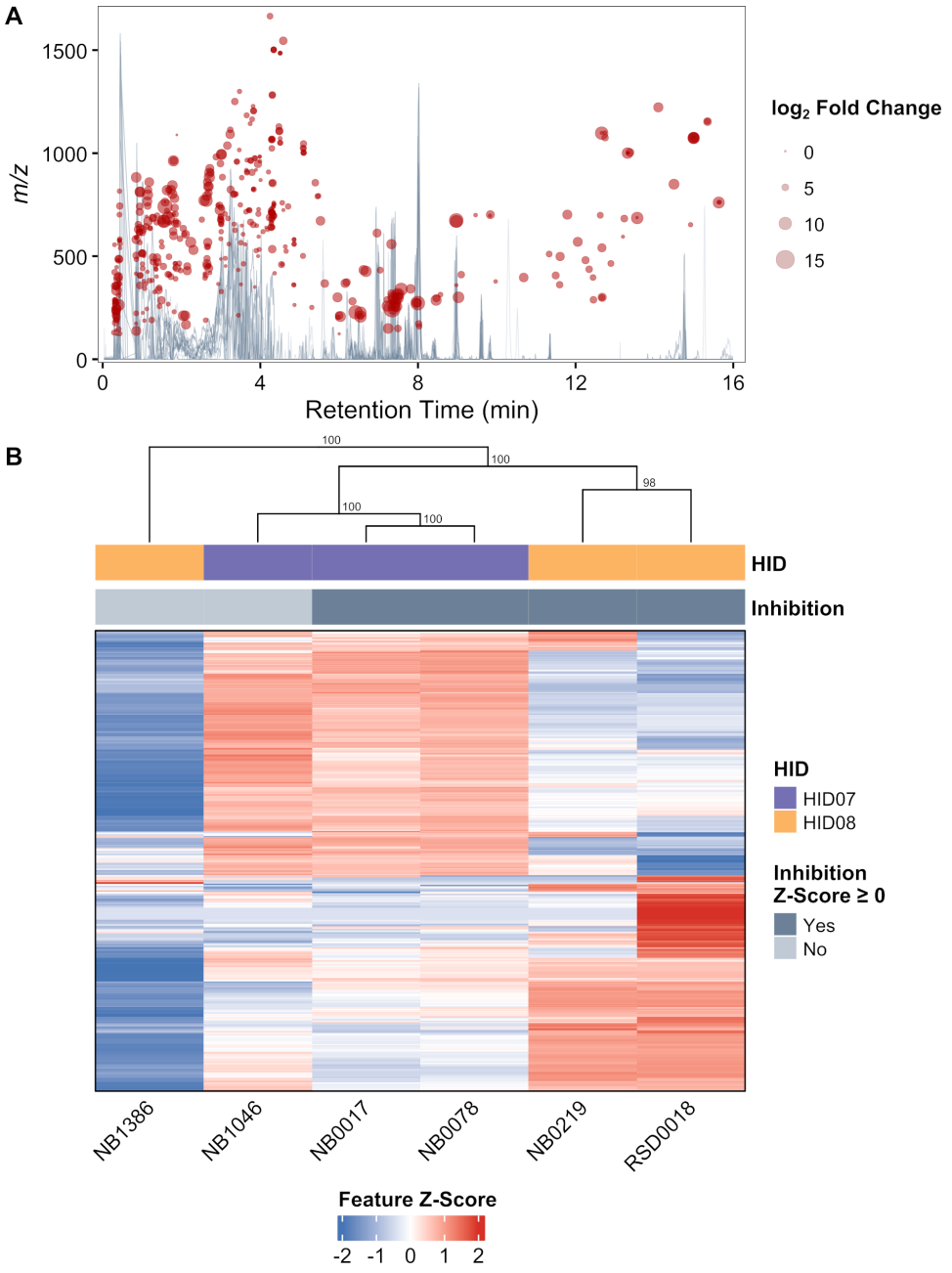


FIG 7 The metabolomes of inhibitory and less-inhibitory *Pseudomonas* isolates are distinct. (A) Cloud plot comparing the metabolome profiles of clinical *Pseudomonas* isolates. Traces represent the total ion chromatograms (TICs) of each of six clinical *Pseudomonas* isolates in triplicate after background subtraction of the mean medium blank. The dark blue and gray TICs are from extracts of inhibitory and less-inhibitory *Pseudomonas* isolates, respectively. Bubbles indicate 468 LC-MS/MS features that differ significantly (Kruskal–Wallis $P \leq 0.01$) across different clinical *Pseudomonas* isolates. The size and shade of each bubble correspond to the $\log_2$ fold change and $-\log_{10} P$ value, respectively, as indicated on the right. (B) Heatmap of the 468 significant features (rows) across the six isolates (columns). The feature intensities were averaged, $\log_2$-transformed, per-feature *Z*-scored, as indicated by the scale below. The isolates were clustered using Euclidean distance and the numbers at each node of the dendrogram represent bootstrap support (pvclust, 1,000 bootstraps). The top color bars represent the donor identity (HID) and inhibitory phenotype, as indicated on the right.

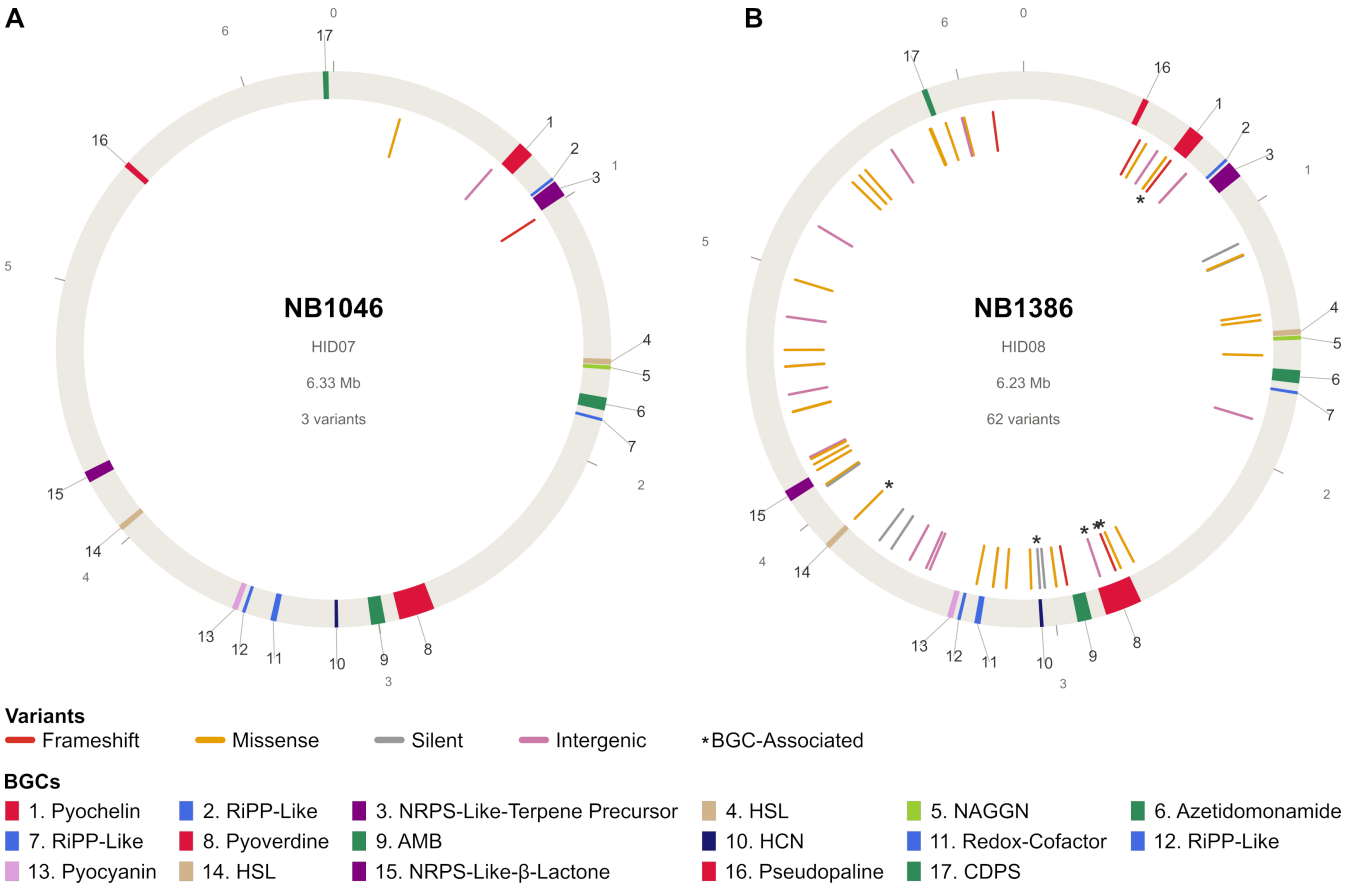


FIG 8 Genomic variation in less-inhibitory *P. aeruginosa* isolates tracks with changes in metabolome profiles. Genome maps of the less-inhibitory *P. aeruginosa* isolates (A) NB1046 and (B) NB1386. The outer gray ring represents the genome with *dnaA* at the 0 position. The light gray numbers on the exterior of the circle indicate chromosomal position in megabase. Ticks on the interior of the circle represent genetic variants in the genome relative to inhibitory isolates from the same donor, and their color represents the type of variant, as indicated by the legend below. BGCs are indicated with color strips and numbered, as indicated by the legend below. Variants that occur within a BGC are marked with an asterisk. Abbreviations: AMB, L-2-amino-4-methoxy-trans-3-butenoic acid; CDPS, tRNA-dependent cyclodipeptide synthase; HCN, hydrogen cyanide; HSL, homoserine lactone; NAGGN, N-acetylglutaminylglutamine amide; NRPS, non-ribosomal peptide synthetase; RIPP, ribosomally synthesized and post-translationally modified peptide.

Genetic differences between inhibitory and less-inhibitory *P. aeruginosa* isolates explain differences in metabolome profiles

We next wanted to identify specific genetic differences between *Pseudomonas* isolates that could explain the variation that we observed in their inhibitory activity and metabolome profiles. As mentioned previously, the metabolomes of the three isolates from HID08 grouped based on inhibition, as expected. In contrast, the metabolome of NB1046 from HID07 grouped with those of the inhibitory isolates, despite being classified as a less-inhibitory isolate, based on the coculture assay. We generated closed genomes using long-read sequencing for each of these six isolates and confirmed that they were all *P. aeruginosa* (average nucleotide identity [ANI] to the type-strain *P. aeruginosa* ATCC 10145^{T}: 99.3%–99.4%). We further determined that each set of three isolates from the same donor likely represent clonal lineages (ANI ≥99.995%) but were distinct between donors (ANI: 99.32%).

We then predicted the secondary metabolite BGC content of each *P. aeruginosa* isolate genome using antiSMASH. Despite the isolates exhibiting variable inhibitory activity in coculture, they all encoded the same 17 BGCs, though 2 of the BGCs (16 and 17) were found in variable chromosomal positions between isolates from the different donors (Fig. 8). This finding prompted us to ask if the metabolomic differences between

Downloaded from https://journals.asm.org/journal/msystems on 06 November 2026 by 139.78.244.80.

these isolates could be explained by single-nucleotide polymorphisms (SNPs), insertions or deletions (indels), or other mutations in the inactive isolates. We identified differences between the isolates and mapped them back to the genome. In total, we only identified seven variants (two SNPs and five indels) between the three isolates from donor HID07 (Fig. 8A; Table S6 in the supplemental material), consistent with more similarity between their metabolomes (Fig. 7B). Specifically, we identified three variants that were unique to isolate NB1046, consisting of a Pro41fs mutation in *mpl* encoding the UDP-MurNAc:L-Ala-γ-D-Glu-meso-DAP ligase, a W275R mutation in a gene encoding a DUF2875-containing protein, and a SNP in an intergenic region. We do not currently understand if or how these variants could affect the inhibitory activity of this isolate. In contrast, we identified 73 variants (55 SNPs, 17 indels, and 1 mixed SNP/indel) between the three isolates from donor HID08, of which 62 were unique to the less-inhibitory NB1386 (Fig. 8B). Notably, isolate NB1386 contained multiple mutations in the BGCs for the siderophores pyoverdine and pyochelin (see Table S7 in the supplemental material). In addition, the less-inhibitory isolate NB1386 possessed multiple additional mutations outside of BGCs that could affect secondary metabolism. For instance, the start codon of *lasI*, which encodes the synthase for the quorum sensing molecule *N*-3-oxododecanoyl homoserine lactone, is mutated to an Ile codon, likely abrogating protein translation. Furthermore, *relA* harbors an in-frame deletion and a missense mutation, and *spoT* has a frameshift, together suggesting loss of the stringent response (see Table S7 in the supplemental material). Both quorum sensing and the stringent response have been previously demonstrated to regulate secondary metabolite production in *P. aeruginosa* (54–56). Together, these data suggest that loss of inhibitory activity in isolate NB1386 and other *Pseudomonas* isolates could be due, in part, to mutations in genes that are essential for secondary metabolite biosynthesis or growth rate control.

DISCUSSION

In this study, we investigated the potential impact of microbial interactions on microbiota dynamics and disease in the airways of pwCF using three levels of interrelated, but independent, evidence: (i) inference of associations between bacteria using microbiome sequencing data, (ii) direct measurement of antagonism between CF bacteria *in vitro*, and (iii) metabolomics and genomics of select *P. aeruginosa* isolates to identify candidate mechanisms underlying variation in inhibitory phenotypes. We initially analyzed preexisting 16S rRNA gene amplicon sequencing data sets, which led us to determine that members of the oropharyngeal microbiota and pathogens exhibit different colonization dynamics within the airways of pwCF (Fig. 1). We then inferred abundance associations that occur between members of these two different groups of bacteria and found that increasing numbers of predicted associations were correlated with higher lung function (Fig. 2). To test the negative abundance associations that we inferred, we performed culture from CF airway specimens to build an isolate library, which we then used for *in vitro* coculture inhibition assays with ecologically relevant bacterial strains. We confirmed that antagonism was widespread among CF isolates (Fig. 3–5). We then noticed that different isolates of *Pseudomonas* possessed variable bioactivity in coculture (Fig. 5 and 6). Finally, we demonstrated that different *P. aeruginosa* isolates, even those from the same person at the same time point, produced different metabolites and exhibited variable bioactivity *in vitro* (Fig. 7 and 8).

Previous studies have reported age-dependent differences in the composition of the CF airway microbiota. It was previously thought that in infancy the airways are colonized primarily by bacteria from the oropharynx and upper respiratory tract (e.g., *Streptococcus* spp. and *Haemophilus influenzae*), followed by an increase in the abundance of *S. aureus* during childhood and adolescence. Finally, *P. aeruginosa* or other rarer pathogens were thought to proliferate in adulthood and as disease advances (7, 51, 57). In our reanalysis of 16S rRNA gene amplicon sequencing studies, we only detected weak age-associated shifts in the composition of the microbiota (see Fig. S2 and S3 in the supplemental material). Accordingly, it has been recently suggested that age-related shifts in pathogen

Downloaded from https://journals.asm.org/journal/msystems on 06 November 2026 by 139.78.244.80.

Downloaded from https://journals.asm.org/journal/msystems on 06 November 2026 by 139.78.244.80.

colonization in the airways of pwCF may largely reflect birth cohort effects, rather than the ecological succession outlined above (58, 59). We were unable to interrogate these effects in our reanalysis due to missing metadata needed to assign birth cohorts. Overall, our data were consistent with broader patterns described in prior work (7, 60), as oropharyngeal bacteria tend to form relatively cohesive communities, whereas pathogens tend to dominate the microbiota when they are present (7, 52, 60). Increased pathogen abundance within the CF airway microbiota was associated with loss of lung function (Fig. 1C and 2C). This pattern could reflect the causal role of pathogens in disease progression but is also consistent with the possibility that the inflammatory and nutrient-rich environment of the CF airway selects for pathogens that are adapted to grow under these conditions (61, 62). Regardless of the direction of this relationship, the association between pathogen abundance and decreased lung function suggests that changes in the structure of the airway microbiota, whether by environmental factors, host immunity, or direct microbial interactions, are linked to disease progression in pwCF.

Reanalysis of 16S rRNA gene amplicon sequencing studies suggested the potential for widespread antagonistic and cooperative interactions among members of the CF airway microbiota (Fig. 2). Notably, we found that increasing numbers of pairs of covarying genera were correlated with higher lung function in pwCF (Fig. 2B). This contrasts with Rivett et al. (13), who recently reported that increasing numbers of coabundant taxa associated with lung function (called "number of interacting taxa" in their paper) were associated with worse disease in the CF airway. These analyses differed in how taxon pairs were chosen. Rivett et al. retained pairs that were already associated with reduced lung function, whereas we selected pairs based on their covariation alone. In our analysis, many of the abundance associations between oropharyngeal genera were positive, and these bacteria are typically associated with a more diverse microbiota and with lung health (8, 18). Our results lead us to hypothesize that the predicted positive associations among oropharyngeal bacteria are characteristic of cohesive communities in healthier pwCF, whereas worse disease is associated with antagonistic interactions involving pathogens that disrupt the microbiota as they become dominant. However, it is important to take care in ascribing ecological interactions to negative associations, especially because relative abundances are composite (i.e., if the relative abundance of one taxon increases, the total relative abundance of all other taxa must decrease). To circumvent these compositional effects, we performed analyses to investigate the effect of pathogens on the structure of the oropharyngeal bacteria community, after we removed reads from pathogens and rarefied the remaining reads to equal depth. This analysis revealed that a pathogen relative abundance of even just 1%–10% reduced the positive associations between the oropharyngeal bacteria by approximately half, which was concomitant with reduced lung health (Fig. 2C). Our interpretation of pathogens disrupting the oropharyngeal microbiota is strengthened by the results of our coculture assays, which found widespread antagonism between pathogens and other respiratory bacteria (Fig. 3) and correlated well with the covariation coefficients from the 16S rRNA gene amplicon sequencing analyses (Fig. 4). This antagonism is also consistent with prior reports that tested smaller numbers of isolates (24). Taken together, these data support a model in which pathogen dominance of the CF airway results from antagonistic interactions that disrupt the oropharyngeal microbiota.

Comparison of the metabolomes (Fig. 7) and genomes (Fig. 8) of *P. aeruginosa* isolates suggests that production of bioactive metabolites is at least, in part, responsible for the ability of these pathogens to antagonize other members of the CF airway microbiota. Notably, several *P. aeruginosa* secondary metabolites have been reported to reach concentrations between 1 and 100 µM in sputum from pwCF (63–65). These concentrations are sufficient to influence the growth of other microbes. However, it is important to note that our current genomic and metabolomic results should be taken as a proof of concept. We have not yet isolated and tested specific compounds produced by *P. aeruginosa* for their bioactivity against CF-associated bacteria or demonstrated that the mutations we identified alter secondary metabolite production. However, if this is the

Downloaded from https://journals.asm.org/journal/msystems on 06 November 2026 by 139.78.244.80.

case, we suspect that other CF pathogens may also produce secondary metabolites that contribute to disruption of the microbiota, but beyond several examples from *Burkholderia* spp. (66–75), not much is known about the compounds produced by other pathogens. It is also important to note that the mechanisms responsible for disruption of the airway microbiota by *P. aeruginosa* and other CF pathogens are likely multifaceted and probably also involve production of secreted enzymes, type VI secretion systems, and other effectors (25). Furthermore, antagonism may not be the only means used by pathogens to become dominant. For example, *Staphylococcus* exhibits dominance in approximately 25% of samples it is detected in (Fig. 1A; Fig. S5 in the supplemental material), yet isolates of *Staphylococcus* were not predicted to be negatively associated with other bacteria (Fig. 2A), and these isolates were largely non-inhibitory (Fig. 5). Whether dominance of the microbiota by *Staphylococcus* is due to priority effects stemming from early colonization, adaptation that promotes survival within the host, or alternative mechanisms will require additional investigation.

The finding of *P. aeruginosa* isolates with variable inhibitory activity from the same donor at the same time point (Fig. 6 to 8) highlights the broad diversification that can occur within pwCF over the course of chronic infection. These observations are consistent with several prior studies that have identified diversification of *P. aeruginosa* that occurs longitudinally within the CF airway (39, 76). In fact, production of the secondary metabolites pyocyanin and pyoverdine has been reported to be lost in *P. aeruginosa* over the course of chronic infection, possibly as an adaptation to surviving in the environment of the CF airway (41, 77). Consistent with these reports, we observed multiple mutations within the pyoverdine BGC within *P. aeruginosa* isolate NB1386. If secondary metabolites are responsible for antagonism, then our results would indicate that these mutations could have consequences for microbial interactions that occur within this environment. Notably, most culture-independent approaches would fail to capture the differences between the isolates that we observed. For instance, 543/558 (97.3%) of the *Pseudomonas* isolates we cultured possess identical 16S rRNA gene V3–V4 region sequences (including the six isolates we characterized using genomics and metabolomics). Thus, use of operational taxonomic units or even amplicon sequence variants would fail to distinguish between these isolates. This observation demonstrates the importance of characterizing multiple isolates from either host or environmental samples to determine how they interact with the host or other members of the community and should be applied more broadly to culture-dependent surveys of other microbial ecosystems.

Here, we note there were limitations in our study. First, due to incomplete metadata and insufficient sampling, it was not possible for us to characterize the CF airway microbiota in a single individual longitudinally to directly observe patterns indicative of microbiota disruption. Due to prior sample preparation protocols that did not limit exposure to oxygen, we were unable to culture strict anaerobes from the donated sputum samples. We predicted multiple abundance associations that involve strictly anaerobic bacteria (Fig. 2A), and it is known that anaerobes play important roles in interactions with CF pathogens (15, 16). In addition, we did not isolate any *Burkholderia* spp., as no sputa were donated from individuals at the Oklahoma City Cystic Fibrosis Clinic that were culture-positive for these pathogens. Second, we have focused exclusively on the bacteria that colonize the airways of pwCF while ignoring *Aspergillus*, *Scedosporium*, and other fungi that often inhabit this same environment. These fungi are known to interact with CF bacteria (19) and to produce bioactive metabolites (78–83). It is also likely that fungi will exhibit isolate-to-isolate variability in their bioactive metabolite production. Furthermore, our cross-streak assays are not well suited to test for positive interactions (e.g., growth promotion) between microbes. While these limitations mean that our cultures are not representative of the overall CF microbiota, to our knowledge they do represent the largest study of interactions between CF microbes to date, and we recapitulate the associations we inferred from amplicon sequencing data (Fig. 4). Finally, our experiments were performed in artificial media and thus do not

fully reflect how the host shapes interspecies interactions in the CF airway (84). Future studies that account for each of these limitations will improve our understanding of the microbial interactions that occur within the CF airway.

In conclusion, our data support a model where *P. aeruginosa* and other CF pathogens may disrupt microbiota structure and dominate the airways, in part through the production of bioactive metabolites, leading to more severe clinical outcomes. We speculate that molecules that target secondary metabolite production by these pathogens could be developed as an antivirulence strategy to keep pathogen proliferation in check and prevent worsening lung disease in pwCF. Furthermore, the isolate-level variability we observed in *P. aeruginosa* indicates that microbial interactions may not be conserved at the same taxonomic resolution where most microbiota surveys are conducted. This finding suggests that characterizing multiple isolates may be necessary to garner a complete picture of the microbial interactions that occur within host and environmental microbiomes.

MATERIALS AND METHODS

Microbiota analyses

We identified 16S rRNA gene amplicon sequencing studies from pwCF by searching the SRA for "cystic fibrosis" AND "16S," followed by manual curation of the resulting studies and cross-validation with the corresponding publications to limit our scope to relevant specimens (i.e., airway, bronchoalveolar lavage, bronchoscope, oropharynx, protected brush, and sputum) (13, 57, 85–120). The inclusion criteria we used were ≥1,000 detected bacterial reads and known sample type. When available, we included the metadata characteristics age, sex, and FEV_1 pp. We obtained these metadata characteristics either from the BioSample directly or by cross-referencing the corresponding publications and/or their supplemental information. In total, we analyzed 5,260 sequencing runs (see Table S1 in the supplemental material for the full list of runs analyzed and the donor demographics). For all analyses, we treated each individual sequencing run as an independent sample. The results from all analyses were consistent when we used linear mixed-effect models with random intercepts for individuals nested within the study or when we restricted multiple samples from the same individual (either by including the sample with the highest number of reads or by pooling all samples per individual).

We downloaded reads from the SRA using fasterq-dump 2.10.3 from the SRA toolkit (https://github.com/ncbi/sra-tools). We then used fastp 0.23.2 (121) for quality control and adapter trimming of the raw reads. To remove potential contamination from human-derived reads, we used bowtie2 2.4.1 and discarded reads that mapped to a reference human genome sequence (GenBank accession number GCA_009914755.4). We then used mothur 1.48.1 (122) to process 16S rRNA gene amplicon sequencing reads and perform taxonomical classification using the Human Oral Microbiome Database 16S rRNA RefSeq v15.23 as the reference (https://www.homd.org//ftp/16S_rRNA_refseq/HOMD_16S_rRNA_RefSeq/V15.23/) (53). We determined the beta diversity by computing Bray–Curtis dissimilarities using the parallelDist package, followed by non-metric multidimensional scaling using the vegan package (123) in R. To test whether microbiota composition differed by host or technical variables, we performed PERMANOVA with the vegan package using 9,999 permutations for the unadjusted models and 999 permutations for all subsequent models. We tested these variables with both unadjusted models and partial models conditioned on the technical covariates (BioProject accession and sample type). For each technical factor (i.e., 16S rRNA gene region, sequencing platform, and sample type), we counted the number of studies that used a single value of that factor (e.g., only one sample type sequenced). We adjusted all PERMANOVA *P* values from the unadjusted models for multiple comparisons using the BH false discovery rate. We report raw permutation *P* values for the partial models. To determine whether effects on microbiota composition were reproducible within studies rather than caused by differences between them, we repeated each partial PERMANOVA with

Downloaded from https://journals.asm.org/journal/msystems on 06 November 2026 by 139.78.244.80.

Downloaded from https://journals.asm.org/journal/msystems on 06 November 2026 by 139.78.244.80.

permutations restricted to within BioProject accessions using the permute package. To account for repeated and longitudinal sampling, we repeated each partial analysis either by restricting it to the sample with the highest bacterial read count per individual or by determining the mean microbiota composition across all samples corresponding to an individual. We then fit unadjusted PERMANOVA separately within each BioProject accession containing ≥20 samples with at least two levels of the variable tested, then determined if the resulting associations agreed between studies. We used a one-way analysis of variance to determine the fraction of variation in $\log_{10}$ sequencing depth explained by BioProject accession. To test whether individual genera were associated with age or lung function, we fit each genus to a separate logistic regression of colonization adults (≥18 years) or children (<18 years) or FEV_1 pp modeled continuously and scaled by 10-point increments. We adjusted both models for BioProject and sample type, and the latter model additionally for age. We corrected *P* values using BH false discovery rate, as above.

We calculated the *H′* for each sample using the vegan package. It is known that measures of FEV_1 vary between researchers, which can have consequences for comparison across studies (124). To account for these potential confounding effects between studies, we adjusted FEV_1 pp using an ordinary least-squares model with covariates of BioProject accession, age, 16S rRNA gene region sequenced, or sample type. We defined FEV_1 pp_{Adj} as the residuals from this model plus the overall mean FEV_1 pp. We excluded any sample from this model that was missing one or more of these covariates. We determined the relationship between *H′* and FEV_1 pp_{Adj} using a linear model adjusting FEV_1 pp for age, BioProject accession, 16S rRNA region sequenced, and sample type. We calculated the BP for each sample as the proportional abundance of the single most abundant genus. We considered samples to be pathogen dominated if the combined relative abundance of the genera *Achromobacter*, *Burkholderia*, *Escherichia*, *Haemophilus*, *Pseudomonas*, *Staphylococcus*, and *Stenotrophomonas* was ≥50% relative abundance. We removed confounding effects of technical factors on BP, as above, for the statistical model.

Covariation analysis

To determine abundance associations between genera in the CF airway microbiota, we applied pairwise linear regression. For these analyses, we only included the genera with an overall metacommunity relative abundance of ≥1.0% and a prevalence of ≥5% across all samples (Table 1). All of our subsequent analyses investigated every unordered pair of these genera ($19 \times 18/2 = 171$ genus pairs). Briefly, we determined all possible pairwise linear regressions between the abundances of two genera (denoted g_1 and g_2) by fitting the ordinary least-squares model: $\log_{10}(g_1 + 1) \sim \log_{10}(g_2 + 1)$ and using the regression slope as a measure of the direction (negative or positive) and magnitude of covariation (i.e., the covariation coefficient). We assessed significance using a Bonferroni-corrected threshold of $\alpha = 0.05/171$. For each sample, we calculated n_g, the number of these significantly covarying pairs in which both genera were detected in that sample at ≥1% relative abundance. To identify which pairs of covarying genera predicted changes in lung function, we fit a linear model for each genus pair using the following model: FEV_1 pp $\sim \log_{10}(g_1 + 1) + \log_{10}(g_2 + 1) + [\log_{10}(g_1 + 1) \times \log_{10}(g_2 + 1)]$. We determined the abundance association term coefficient and *P* value for each pair of covarying genera and corrected for multiple hypothesis testing using the BH FDR. We then tested the association between n_g and lung function while controlling for confounders by fitting a multiple regression: FEV_1 pp $\sim n_g$ + age + BioProject accession + 16S rRNA gene region sequenced + sample type. We adjusted each FEV_1 pp for these confounders using the residuals plus the mean, as above. We generated bootstrap confidence bands from 100 resampled trend lines.

To test how pathogen relative abundance influenced covariation among oropharyngeal bacteria, we performed an alternative version of the above analysis. We binned groups based on the relative abundance of pathogens, then removed the

pathogens from the abundance matrix, which retained 4,170 samples with ≥1,000 reads from oropharyngeal bacteria. Over 2,000 bootstrap draws, we resampled each bin with replacement, rarefied each sample to 1,000 oropharyngeal bacterial reads, and calculated covariation for all 66 oropharyngeal bacterial genus pairs, as above. We compared bins using the bootstrap distributions of their differences with BH correction. The percentage of samples with high lung function (defined as FEV_1 pp ≥80) was calculated within the same pathogen relative abundance bins and bootstrapped identically.

Isolation and maintenance of bacteria from CF samples

Sputum and oropharyngeal samples from 96 pediatric and adult pwCF at the Oklahoma Cystic Fibrosis Clinic were previously collected and stored in the laboratory of Dr. Erika Lutter (see Table S4 in the supplemental material for donor information). Sputum samples were collected from patients by the clinical staff in 50 mL sterile conical tubes. The clinic staff provided information on the patient age, gender, and medical condition upon admittance to the clinic, and a deidentified number was assigned to each sample. These samples were then cultured on non-selective brain–heart infusion (BHI; 0.6% [wt/vol] brain heart infusion, 0.6% [wt/vol] peptic digest of animal tissue, 0.5% sodium chloride [NaCl], 0.3% [wt/vol] dextrose, 1.45% [wt/vol] pancreatic digest of gelatin, 0.25% [wt/vol] disodium phosphate, 1.5% [wt/vol] agar) or skim milk (10% [wt/vol] skim milk, 1.5% [wt/vol] agar) plates aerobically at 37°C for 3 days. Afterward, these plates were scraped, and all bacterial biomass was cryopreserved at −80°C in 10% (wt/vol) skim milk. We generated an isolate library by streaking these samples onto the following differential and selective media at 37°C for approximately 1 week:

Burkholderia cepacia selective agar (1.0% [wt/vol] casein peptone, 1.0% [wt/vol] lactose, 1.0% [wt/vol] sucrose, 0.5% [wt/vol] sodium chloride, 226 µM phenol red, 1.5% [wt/vol] agar, with the following additions after autoclaving: 5 µM crystal violet, 10 µg/mL gentamicin, 2.5 µg/mL vancomycin, 60 µg/mL polymyxin B, pH 7.0); cetrimide agar (2.0% [wt/vol] gelysate peptone, 0.14% [wt/vol] magnesium chloride, 1.0% [wt/vol] potassium sulfate, 0.03% [wt/vol] cetrimide, 1% [vol/vol] glycerol, 1.5% [wt/vol] agar, pH 7.2); eosin methylene blue (1.0% [wt/vol] gelatin peptone, 1.0% [wt/vol] lactose, 0.2% [wt/vol] dipotassium hydrogen phosphate, 0.04% [wt/vol] eosin yellow, 0.0065% [wt/vol] methylene blue, 1.5% [wt/vol] agar, pH 7.1); *Haemophilus* isolation agar (1.6% [wt/vol] casein peptone, 0.5% [wt/vol] sodium chloride, 0.5% [wt/vol] protease peptone, 0.8% [wt/vol] BHI, 0.2% [wt/vol] dextrose, 0.25% [wt/vol] disodium phosphate, 1.5% [wt/vol] agar, with the following additions after autoclaving: 109 µM nicotinamide adenine dinucleotide, ≥8,250 U bacitracin, 10 mg hemin, and 5.0% [vol/vol] defibrinated horse blood, pH 7.3); LBVT.SNR (1.0% [wt/vol] tryptone, 0.5% [wt/vol] yeast extract, 0.5% [wt/vol] sodium chloride, 1 mM sodium hydroxide, 86 µM neutral red, 1.5% [wt/vol] agar, with the following additions after autoclaving: 1.0% wt/vol sucrose, 3 µg/mL vancomycin, and 3 µg/mL trimethoprim); mannitol soy agar (1.0% [wt/vol] protease peptone, 0.1% [wt/vol] beef extract, 7.5% [wt/vol] sodium chloride, 1.0% [wt/vol] D-mannitol, 70 µM phenol red, and 1.5% [wt/vol] agar, pH 7.4), MacConkey media (1.7% [wt/vol] gelatin peptone, 1.0% [wt/vol], sodium chloride, 0.15% [wt/vol] bile salts, 0.15% [wt/vol] casein peptone, 0.15% [wt/vol] meat peptone, 104 µM neutral red, 2.5 µM crystal violet, 1.35% [wt/vol] agar, pH 7.1) supplemented with 0.5% [wt/vol] lactose (MCL) or 0.5% [wt/vol] xylose with the following additions after autoclaving: 20 µg/mL vancomycin, 20 µg/mL aztreonam, and 5 µg/mL amphotericin B; Mitis-Salivarius agar with Tellurite (5.0% [wt/vol] sucrose, 1.0% [wt/vol] proteose peptone, 1.0% [wt/vol] tryptose, 0.4% [wt/vol] dipotassium phosphate, 0.1% [wt/vol] dextrose, 78 µM trypan blue, 2.0 µM crystal violet, 1.5% [wt/vol] agar, with the following addition after autoclaving: 0.001% [wt/vol] potassium tellurite, pH 7.0); *Rothia* enrichment medium agar (2.5% [wt/vol] heart infusion, 1.5% [wt/vol] agar, with the following additions after autoclaving: 10 µg/mL colistin and 0.5 µg/mL lincomycin).

We used GasPak jars containing carbon dioxide generators (BD), as necessary, for anaerobic incubation. We selected ≥2 colonies of each distinct morphology per sample

Downloaded from https://journals.asm.org/journal/msystems on 06 November 2026 by 139.78.244.80.

per media type and passaged the strains aerobically on BHI agar plates to obtain pure cultures. We preserved all isolates at −80°C in 25% (vol/vol) glycerol. We provide details for all bacterial isolates used in this study in Table S5 in the supplemental material. For general propagation and manipulation, we cultured bacterial isolates on BHI agar plates or in BHI broth aerobically at 37°C with shaking.

Identification of bacterial isolates

Identification of all bacterial isolates was performed via colony PCR and high-throughput sequencing in 96-sample batches at the Oklahoma State University Microbiomics and Culturomics Core Facility. Briefly, single bacterial colonies on BHI agar plates were touched with a pipette tip and resuspended in 20 µL sterile, nuclease-free water heated at 95°C for 10 min. The 16S rRNA gene V3-V4 region was amplified using primers 341F (5′-[Illumina Adapter]-[6 nucleotide randomized tag]-CCTACGGGNGGCWGCAG-3′) and 805R (5′-[Illumina Adapter]-[6 nucleotide randomized tag]-GACTACHVGGGTATCTAATCC -3′). Each 25 µL reaction mixture contained 3 µL lysate, 20 pmol of each primer, and 12.5 µL of DreamTaq 2× Master Mix (Thermo Scientific) with the following PCR cycling conditions: 95°C for 2 min; 25 cycles at 95°C for 30 s, 55°C for 30 s, and 72°C for 30 s; and a final extension at 72°C for 5 min. PCR amplification was confirmed for all samples using 1.0% (wt/vol) agarose tris-acetate-EDTA (TAE) gels.

Subsequently, a Research Silicon-A Plate Kit (Zymo Research) was used for PCR cleanup following the manufacturer's instructions. Nextera XT DNA library preparation kits (Illumina) were used for library preparation. Each 25 µL reaction mixture contained 5 µL of cleaned PCR product, 2.5 µL i7, 2.5 µL i5, and 12.5 µL 2× Master Mix with the following PCR cycling conditions: 95°C for 3 min; eight cycles at 95°C for 30 s, 55°C for 30 s, and 72°C for 30 s; and a final extension at 72°C for 5 min. As before, PCR amplification was confirmed using TAE gels. These samples were then cleaned using a ratio of 1:0.6 volume sample to AMPure XP magnetic beads (Beckman Coulter). The beads and samples were incubated for 5–8 min at ambient temperature, washed twice with 200 µL of 80% (vol/vol) ethanol, air dried for 3–5 min, and eluted with 50 µL of 10 mM Tris-HCl, pH 8.5. The libraries were quantified using a Qubit dsDNA HS fluorometer (Invitrogen) and normalized to an equal molar concentration and pooled per 384-sample batch. The libraries were then sequenced using a NextSeq 2000 P1 600 Cycle (2 × 300 bp), following the platform loading guidance.

The pooled sequencing reads were demultiplexed into per-colony FASTQ files, and basic read processing was performed using mothur, as above. We used the classify.seqs function in mothur to identify isolates using the eHOMD 16S rRNA RefSeq v15.23 (53) with an 80% bootstrap confidence cutoff. If we failed to obtain a PCR product from the high-throughput colony PCR method, we then performed targeted colony PCR and Sanger sequencing. The identities of these isolates are provided in Table S5 in the supplemental material.

Cross-streak assays

We inoculated 3 mL BHI broth with single colonies of CF bacterial isolates and incubated the cultures at 37°C overnight with shaking. We then spread 20 µL of the undiluted overnight culture in a ~8 × ~1.5 cm-wide line in the center of a 25 mL BHI agar plate (diameter: 8.6 cm). We incubated the plates aerobically for 18–20 h at 37°C. We prepared overnight (16–18 h) cultures of *A. xylosoxidans* subsp. *xylosoxidans* strain DSM 2402, *B. cenocepacia* strain K56-2, *B. cepacia* strain DSM 7288, *N. meningitidis* strain DSM 10036, *P. aeruginosa* strain PID25, *R. mucilaginosa* strain HM-1055, and *S. aureus* strain PID40 by inoculating single colonies into 3 mL BHI broth and incubating cultures at 37°C with shaking. We prepared cultures of *S. oralis* subsp. *oralis* strain DSM 20627 in tryptone soy broth (1.7% [wt/vol] pancreatic digest of casein, 0.3% [wt/vol] papaic digest of soybean, 0.25% [wt/vol] dextrose, 0.5% [wt/vol] NaCl, 0.25% [wt/vol] dipotassium phosphate) overnight at 37°C statically. Subsequently, with the exception of *S. oralis* subsp. *oralis*, we diluted these cultures 10-fold in BHI and then used wooden applicator sticks to streak the

Downloaded from https://journals.asm.org/journal/msystems on 06 November 2026 by 139.78.244.80.

cultures perpendicularly to the original isolate streak. We used the *S. oralis* subsp. *oralis* culture directly without dilution. We then returned the plates to 37°C and measured the ZOI after overnight incubation. For each set of assays, we inoculated the target strains on a BHI plate without a CF isolate as a control to verify culture viability and purity. Due to the large number of isolates tested in this study, we did not replicate cross-streak assays.

We used ImageJ (125) to measure the ZOI, which we defined as the distance from the original isolate streak to the point at which the target organism began to grow. If a target was not inhibited, we scored the interaction as no inhibition (ZOI = 0 cm). If a target failed to grow on the coculture plate but grew well on the control plate, we scored the interaction as strong inhibition (ZOI ≥2 cm). We did not score interactions where there was poor growth of the target strain on the control plate or visible contamination of either the isolate or target streak. For consistency, all ZOIs were measured by S.M.M. and spot-checked by R.M.S.

To test whether inhibition differed by target or genus of CF isolate, we performed χ^2 tests of independence and estimated *P* values by Monte Carlo simulation (B = 100,000 replicates). To quantify the overall inhibitory activity of individual isolates, we computed the sum inhibition score of each isolate against all eight targets (range: 0–24) and then applied *Z*-score normalization. We limited this analysis to only the 1,364 isolates that were tested successfully against all eight targets. We determined differences in *Z*-scores across the genera using the Kruskal–Wallis rank-sum test with post hoc pairwise Wilcoxon rank-sum tests with BH correction for multiple comparisons. We assessed the equality of variance in *Z*-scores using the Fligner–Killeen test with BH correction for multiple comparisons.

Characterization of *P. aeruginosa* metabolomes

We inoculated 3 mL BHI with *Pseudomonas* isolates at an initial OD_{600} of 0.0003 and cultured them aerobically at 37°C for 24 h with shaking. Afterward, we removed cells from 2 mL of culture via centrifugation at 21,130 × *g* for 20 min at ambient temperature. We stored 200 µL aliquots at −20°C. We transferred the remaining 1.8 mL of CFS into glass scintillation vials and treated them with three to four drops of chloroform to kill any remaining cells and then evaporated them *in vacuo* using a Biotage V-10 Touch system. We stored the dried CFS at −20°C until processing. To test the CFS for activity, we diluted an overnight cultures of that target strains to an OD_{600} between 0.01 and 0.001, depending on the strain, and spread 200 µL onto a one-well dish containing 35 mL BHI agar. We then thawed CFS, centrifuged them at 21,130 × *g* for 5 min at 4°C, spotted 5 µL onto the plate with the target strains, and incubated the culture at 37°C for 24 h before scoring inhibition by identifying ZOIs visually.

We resuspended the dried CFS to 1 mg/mL in MilliQ water, diluted them to 0.1 mg/mL, and injected 2 µL for LC-MS/MS analysis. We obtained high-resolution mass spectrometry data using an Agilent 1260 HPLC consisting of a degasser, quaternary pump, autosampler, and column compartment upstream of an Agilent 6545 Q-ToF. Separation was achieved using a Kinetex C18 column (50 × 2.1 mm, 100 Å, 2.6 µm; Phenomenex, Torrance, CA) at a flow rate of 0.4 mL/min, held at 30°C. Line C was water with 0.1% (vol/vol) formic acid, and line D was acetonitrile with 0.1% (vol/vol) formic acid. The column was preequilibrated with 97% C/3% D. Upon injection, the mobile phase composition was maintained for 0.75 min, followed by changing the mobile phase to 10% C/90% D over 9.5 min using a linear gradient. Over the next 0.1 min, the mobile phase was changed to 100% D, and this composition was held for 3.65 min. The mobile phase was changed to 97% C/3% D over 0.5 min and held for an additional 1.5 min. The mobile phase was held at 97% C/3% D for an additional 3.5 min prior to injection of the next sample. The Agilent Q-ToF mass spectrometer was equipped with an Agilent JetSpray source operated with the following parameters: auto MS/MS mode, positive polarity; gas temp, 325°C; drying gas, 10 L/min; nebulizer, 20 psi; sheath gas temp, 375°C; sheath gas flow, 12 L/min; VCap, 4,000 V; nozzle voltage (expt), 600 V; fragmentor, 175 V; skimmer, 65 V; Oct 1 RF Vpp, 750 V; mass range, 100–3,000 *m/z*; acquisition rate, 10

Downloaded from https://journals.asm.org/journal/msystems on 06 November 2026 by 139.78.244.80.

spectra/s; and time, 100 ms/spectrum. The MS/MS spectra (five most intense ions) were obtained by data-dependent acquisition with the following parameters, isolating the precursor *m*/z with a medium isolation width (4 *m*/z), summing spectra generated with collision energies of 20, 40, and 60.

We converted raw LC-MS/MS data to .mzXML files using msconvert v3.0.23016 and uploaded them to the XCMS Online server (126). We processed analyses using the multigroup analysis feature and sample data using the standard HPLC/Q-ToF settings with the following parameters: feature detection: method, centWave; ppm, 30; minimum peak width, 10; maximum peak width, 60; signal/noise threshold, 6; mzdiff, 0.01; integration method, 2; prefilter peaks, 3; prefilter intensity, 500; and noise filter, 0; retention time correction: method, obiward; profStep, 0.5; alignment: bw, 5; minfrac, 0.5; mzwid, 0.025; min samp, 1; max, 100; statistics: statistical test, Kruskal–Wallis non-parametric; performed paired test, view pairs 1; performed post hoc analysis, true; *P* value threshold, 0.01; fold-change threshold, 1.5; *P* value threshold, 0.01; value, into; normalization, none; annotation: ppm, 5; *m/z* absolute error, 0.015; search for, isotopes; identification: ppm, 100; adducts, $[M + H]^+$; sample biosource, none; pathway ppm deviation, 5; input intensity threshold, 0; significant list *P* value cutoff, auto; visualization: EIC width, 200; miscellaneous: correct mass calibration gaps, no; bypass file sanity check, no.

We performed all downstream analyses on the 468 features that differed significantly across isolates (Kruskal–Wallis $P \leq 0.01$). For each significant feature, we calculated a multigroup fold change as the ratio of the largest to the smallest non-zero class-mean intensity. We background-corrected the total ion chromatogram (TIC) of every non-blank injection by subtracting the mean TIC of BHI medium blanks, and set any resulting negative values to zero. For hierarchical analysis, we averaged triplicate biological replicates of each isolate to yield a single intensity profile per isolate, $\log_2$-transformed the profiles, and standardized each feature to a *Z*-score across isolates. We then clustered profiles by Euclidean distance with complete linkage and estimated support for the clustering by multiscale bootstrap resampling of the features using pvclust (127) with 1,000 bootstrap replicates. To evaluate the contributions of donor and inhibitory phenotype to variation in the metabolome, we corrected the same significant features for medium background by subtracting the mean intensity of the BHI blanks from each feature and setting negative values to zero. We then normalized the blank-corrected intensities to a constant total ion current per sample using total-sum scaling, computed pairwise Bray–Curtis dissimilarities, and fit PERMANOVA models, as above, with donor and inhibitory phenotype specified as marginal terms and using 9,999 permutations. We summarized each term using the ω^2 effect size. We ordinated the samples by principal coordinate analysis and plotted the first two axes.

Genomic DNA extraction and sequencing of *P. aeruginosa* isolates

We extracted genomic DNA from *P. aeruginosa* isolates using a previously reported method (128). Briefly, we washed cell pellets from 3 mL of an overnight culture in BHI broth in 1 mL of buffer 1 (150 mM NaCl, 10 m M EDTA, 20 mM Tris-HCl, pH 8). We then resuspended the cells in 1 mL of fresh buffer 1 with 1 mg RNase A and SDS to a final concentration of 1.4% (wt/vol). We incubated the samples at 37°C for 90 min. We then added 0.4 mg of proteinase K and incubated samples at 65°C for 20 min. We then incubated samples at 37°C for 16 h to ensure complete lysis. Subsequently, we extracted and purified genomic DNA used standard phenol-chloroform extraction and precipitation with isopropanol. We submitted genomic DNA to Plasmidsaurus for whole genome sequencing using Oxford Nanopore Technology. Libraries were prepared using v14 library prep chemistry and sequenced using a R10.4.1 flow cells. Bases were called using Dorado v4.3 with default Q10 quality filtering (https://github.com/nanoporetech/dorado). Then, Filtlong v0.2.1 (https://github.com/rrwick/Filtlong) was used to remove reads <300 bp and retain the 95% highest quality reads. Subsequently, Autocycler (129) was used to generate assemblies with Flye v2.9.6+ (130) and Hifiasm (131), remove low depth and small contigs, then compress, cluster, trim and, resolve the

Downloaded from https://journals.asm.org/journal/msystems on 06 November 2026 by 139.78.244.80.

assemblies. We provide all genome assembly statistics in Table S8 in the supplemental material.

Genome analyses

We computed ANI among the six isolates and the reference *P. aeruginosa* strain ATCC 10145^T (accession number NZ_CP012001.1) using fastANI v1.33 (132). We annotated each genome with Batka v1.8.1 (133) using the following parameters: --genus Pseudomonas --species aeruginosa --complete. We predicted BGCs in each genome with antiSMASH v8.0.4 (134) using the following parameters: --cb-knownclusters --cc-mibig. We identified variants in the isolate genomes using Snippy v4.6.0 (https://github.com/tseemann/snippy). We considered any variant that fell within BGC predicted by antiSMASH to be BGC associated.

Statistical analysis and data visualization

We performed all statistical analyses in R with specific packages as described in the preceding sections. We generated graphics using ggplot2 (135) with some cleanup and figure assembly in InkScape.

Downloaded from https://journals.asm.org/journal/msystems on 06 November 2026 by 139.78.244.80.

ACKNOWLEDGMENTS

We thank Elixiva Marcum, Josie Hayes, and Helen Zagloul (Oklahoma State University [OSU]) for assistance with experiments related to this project. We thank Mostafa Elshahed, Sam Miller, and Aymen Yassir (OSU Microbiomics and Culturomics Core Facility) for sequence identification of isolates (P20 GM152333). We thank Paul Lawson (University of Oklahoma) and Matthew Traxler (University of California, Berkeley) for suggestions on the research. We thank Tyrrell Conway (OSU) for comments on the manuscript. We thank our anonymous reviewers for providing feedback that substantially improved the manuscript. We thank all individuals who provided samples for our study, as well as those who contributed samples to the studies we reanalyzed, and the researchers whose data we reanalyzed.

This work was supported by the National Institute of General Medical Sciences Centers of Biomedical Research Excellence program (P20 GM152333), by startup funds from Oklahoma State University awarded to R.M.S., and by internal research funding from Oregon State University awarded to B.P. S.S. was supported by T32AT010131 (awarded to Drs. Mahmud and van Breemen, Oregon State University). The Agilent QTOF instrument used in this study was purchased with funds from the Division of Research and Innovation and College of Pharmacy at Oregon State University. The funders had no role in study design, data collection and interpretation, or the decision to submit the work for publication.

AUTHOR AFFILIATIONS

[1]Department of Microbiology and Molecular Genetics, Oklahoma State University, Stillwater, Oklahoma, USA
[2]Department of Pharmaceutical Sciences, Oregon State University, Corvallis, Oregon, USA

AUTHOR ORCIDs

Erika I. Lutter http://orcid.org/0000-0002-1953-2467
Benjamin Philmus http://orcid.org/0000-0003-2085-0873
Reed M. Stubbendieck http://orcid.org/0000-0003-1507-3272

FUNDING

Funder	Grant(s)	Author(s)
National Institute of General Medical Sciences	P20 GM152333	Reed M. Stubbendieck
National Center for Complementary and Integrative Health	T32AT010131	Shaz Sutherland

AUTHOR CONTRIBUTIONS

Sydney M. Morabbi, Data curation, Formal analysis, Investigation | Niladri Bhowmik, Data curation, Formal analysis, Investigation | Shaz Sutherland, Data curation, Formal analysis, Investigation | Evelyn A. Wylie, Investigation | Reagan S. Decker, Investigation | Akram Al Daerwish, Investigation | Mercedes Pérez Pérez, Investigation | Elizabeth Pascual, Investigation | Erika I. Lutter, Resources | Benjamin Philmus, Data curation, Formal analysis, Funding acquisition | Reed M. Stubbendieck, Conceptualization, Data curation, Formal analysis, Funding acquisition, Investigation, Supervision, Visualization, Writing – original draft, Writing – review and editing, Resources

DATA AVAILABILITY

16S rRNA gene amplicon sequencing data were downloaded from the SRA. Metadata and accession numbers for these runs are provided in Table S1. The processed amplicon sequences generated for bacteria isolated for this study are deposited in GenBank under accession numbers PZ656496–PZ658092. The genome sequences for *P. aeruginosa* isolates are available under BioProject accession number PRJNA1491524. The raw mass spectrometry data are deposited at MassIVE under accession number MSV000102457. All other raw data and derived data are available at https://doi.org/10.6084/m9.figshare.32939627. The scripts necessary to replicate this work are available at https://github.com/reedstubbendieck/CF_Interactions.

ETHICS APPROVAL

This study was deemed "not human subjects research" by the University of Oklahoma Institutional Review Board.

ADDITIONAL FILES

The following material is available online.

Supplemental Material

Supplemental Figures (mSystems01157-26-s0001.pdf). Figures S1 to S7.
Captions (mSystems01157-26-s0002.docx). Supplemental table captions.
Table S1 (mSystems01157-26-s0003.csv). Accessions and metadata for amplicon sequencing samples analyzed in this study.
Table S2 (mSystems01157-26-s0004.csv). Effects of clinical and sample variables on CF airway microbiota composition.
Table S3 (mSystems01157-26-s0005.csv). Per-study reproducibility of clinical and sample variables on CF airway microbiota composition.
Table S4 (mSystems01157-26-s0006.csv). Metadata and demographics for donors included in this study.
Table S5 (mSystems01157-26-s0007.csv). Identification of CF isolates used in this study.
Table S6 (mSystems01157-26-s0008.csv). Genetic variation in *P. aeruginosa* isolates from donor HID07.
Table S7 (mSystems01157-26-s0009.csv). Genetic variation in *P. aeruginosa* isolates from donor HID08.
Table S8 (mSystems01157-26-s00010.csv). Genome assembly statistics for *P. aeruginosa* isolates sequenced as part of this study.

Downloaded from https://journals.asm.org/journal/msystems on 06 November 2026 by 139.78.244.80.

REFERENCES

1. Pillai RS, Chandra T, Miller IF, Lloyd-Still J, Yeates DB. 1992. Work of adhesion of respiratory tract mucus. J Appl Physiol (1985) 72:1604–1610. https://doi.org/10.1152/jappl.1992.72.4.1604
2. Button B, Goodell HP, Atieh E, Chen Y-C, Williams R, Shenoy S, Lackey E, Shenkute NT, Cai L-H, Dennis RG, Boucher RC, Rubinstein M. 2018. Roles of mucus adhesion and cohesion in cough clearance. Proc Natl Acad Sci USA 115:12501–12506. https://doi.org/10.1073/pnas.1811787115
3. Elborn JS. 2016. Cystic fibrosis. Lancet 388:2519–2531. https://doi.org/10.1016/S0140-6736(16)00576-6
4. O'Toole GA. 2018. Cystic fibrosis airway microbiome: overturning the old, opening the way for the new. J Bacteriol 200:e00561-17. https://doi.org/10.1128/JB.00561-17
5. Moore JE, Shaw A, Millar BC, Downey DG, Murphy PG, Elborn JS. 2005. Microbial ecology of the cystic fibrosis lung: does microflora type influence microbial loading? Br J Biomed Sci 62:175–178. https://doi.org/10.1080/09674845.2005.11732707
6. Guss AM, Roeselers G, Newton ILG, Young CR, Klepac-Ceraj V, Lory S, Cavanaugh CM. 2011. Phylogenetic and metabolic diversity of bacteria associated with cystic fibrosis. ISME J 5:20–29. https://doi.org/10.1038/ismej.2010.88
7. Coburn B, Wang PW, Diaz Caballero J, Clark ST, Brahma V, Donaldson S, Zhang Y, Surendra A, Gong Y, Elizabeth Tullis D, Yau YCW, Waters VJ, Hwang DM, Guttman DS. 2015. Lung microbiota across age and disease stage in cystic fibrosis. Sci Rep 5:10241. https://doi.org/10.1038/srep10241
8. Adekoya AE, Kargbo HA, Ibberson CB. 2023. Defining microbial community functions in chronic human infection with metatranscriptomics. bioRxiv:2023.06.06.543868. https://doi.org/10.1101/2023.06.06.543868
9. Zhao CY, Hao Y, Wang Y, Varga JJ, Stecenko AA, Goldberg JB, Brown SP. 2021. Microbiome data enhances predictive models of lung function in people with cystic fibrosis. J Infect Dis 223:S246–S256. https://doi.org/10.1093/infdis/jiaa655
10. Varga JJ, Zhao CY, Davis JD, Hao Y, Farrell JM, Gurney JR, Voit E, Brown SP. 2022. Antibiotics drive expansion of rare pathogens in a chronic infection microbiome model. mSphere 7:e0031822. https://doi.org/10.1128/msphere.00318-22
11. Harrison F. 2007. Microbial ecology of the cystic fibrosis lung. Microbiology 153:917–923. https://doi.org/10.1099/mic.0.2006/004077-0
12. Jean-Pierre F, Vyas A, Hampton TH, Henson MA, O'Toole GA. 2021. One versus many: polymicrobial communities and the cystic fibrosis airway. mBio 12:e00006-21. https://doi.org/10.1128/mBio.00006-21
13. Rivett DW, Hatfield LR, Gavillet H, Hardman M, van der Gast C. 2025. Bacterial interactions underpin worsening lung function in cystic fibrosis-associated infections. mBio 16:e0145624. https://doi.org/10.1128/mbio.01456-24
14. Camus L, Briaud P, Vandenesch F, Moreau K. 2021. How bacterial adaptation to cystic fibrosis environment shapes interactions between *Pseudomonas aeruginosa* and *Staphylococcus aureus*. Front Microbiol 12:617784. https://doi.org/10.3389/fmicb.2021.617784
15. Flynn JM, Niccum D, Dunitz JM, Hunter RC. 2016. Evidence and role for bacterial mucin degradation in cystic fibrosis airway disease. PLoS Pathog 12:e1005846. https://doi.org/10.1371/journal.ppat.1005846
16. Flynn JM, Cameron LC, Wiggen TD, Dunitz JM, Harcombe WR, Hunter RC. 2020. Disruption of cross-feeding inhibits pathogen growth in the sputa of patients with cystic fibrosis. mSphere 5:e00343-20. https://doi.org/10.1128/mSphere.00343-20
17. Silveira CB, Cobián-Güemes AG, Uranga C, Baker JL, Edlund A, Rohwer F, Conrad D. 2021. Multi-omics study of keystone species in a cystic fibrosis microbiome. Int J Mol Sci 22:12050. https://doi.org/10.3390/ijms222112050
18. Muhlebach MS, Hatch JE, Einarsson GG, McGrath SJ, Gilipin DF, Lavelle G, Mirkovic B, Murray MA, McNally P, Gotman N, Davis Thomas S, Wolfgang MC, Gilligan PH, McElvaney NG, Elborn JS, Boucher RC, Tunney MM. 2018. Anaerobic bacteria cultured from cystic fibrosis airways correlate to milder disease: a multisite study. Eur Respir J 52:1800242. https://doi.org/10.1183/13993003.00242-2018
19. Granchelli AM, Adler FR, Keogh RH, Kartsonaki C, Cox DR, Liou TG. 2018. Microbial interactions in the cystic fibrosis airway. J Clin Microbiol 56:e00354-18. https://doi.org/10.1128/JCM.00354-18
20. Filkins LM, Graber JA, Olson DG, Dolben EL, Lynd LR, Bhuju S, O'Toole GA. 2015. Coculture of *Staphylococcus aureus* with *Pseudomonas aeruginosa* drives *S. aureus* towards fermentative metabolism and reduced viability in a cystic fibrosis model. J Bacteriol 197:2252–2264. https://doi.org/10.1128/JB.00059-15
21. Bernardy EE, Raghuram V, Goldberg JB. 2022. *Staphylococcus aureus* and *Pseudomonas aeruginosa* isolates from the same cystic fibrosis respiratory sample coexist in coculture. Microbiol Spectr 10:e0097622. https://doi.org/10.1128/spectrum.00976-22
22. Kvich L, Crone S, Christensen MH, Lima R, Alhede M, Alhede M, Staerk D, Bjarnsholt T. 2022. Investigation of the mechanism and chemistry underlying *Staphylococcus aureus'* ability to inhibit *Pseudomonas aeruginosa* growth *in vitro*. J Bacteriol 204:e0017422. https://doi.org/10.1128/jb.00174-22
23. Scott JE, Li K, Filkins LM, Zhu B, Kuchma SL, Schwartzman JD, O'Toole GA. 2019. *Pseudomonas aeruginosa* can inhibit growth of streptococcal species via siderophore production. J Bacteriol 201:1–18. https://doi.org/10.1128/JB.00014-19
24. Menetrey Q, Dupont C, Chiron R, Jumas-Bilak E, Marchandin H. 2020. High occurrence of bacterial competition among clinically documented opportunistic pathogens including *Achromobacter xylosoxidans* in cystic fibrosis. Front Microbiol 11:558160. https://doi.org/10.3389/fmicb.2020.558160
25. Stubbendieck RM, Straight PD. 2016. Multifaceted interfaces of bacterial competition. J Bacteriol 198:2145–2155. https://doi.org/10.1128/JB.00275-16
26. Stubbendieck RM, Vargas-Bautista C, Straight PD. 2016. Bacterial communities: interactions to scale. Front Microbiol 7:1234. https://doi.org/10.3389/fmicb.2016.01234
27. Stubbendieck RM, Zelasko SE, Safdar N, Currie CR. 2021. Biogeography of bacterial communities and specialized metabolism in human aerodigestive tract microbiomes. Microbiol Spectr 9:e0166921. https://doi.org/10.1128/Spectrum.01669-21
28. Lau GW, Ran H, Kong F, Hassett DJ, Mavrodi D. 2004. *Pseudomonas aeruginosa* pyocyanin is critical for lung infection in mice. Infect Immun 72:4275–4278. https://doi.org/10.1128/IAI.72.7.4275-4278.2004
29. Allen L, Dockrell DH, Pattery T, Lee DG, Cornelis P, Hellewell PG, Whyte MKB. 2005. Pyocyanin production by *Pseudomonas aeruginosa* induces neutrophil apoptosis and impairs neutrophil-mediated host defenses *in vivo*. J Immunol 174:3643–3649. https://doi.org/10.4049/jimmunol.174.6.3643
30. Hao Y, Kuang Z, Xu Y, Walling BE, Lau GW. 2013. Pyocyanin-induced mucin production is associated with redox modification of FOXA2. Respir Res 14:82. https://doi.org/10.1186/1465-9921-14-82
31. Jo J, Price-Whelan A, Cornell WC, Dietrich LEP. 2020. Interdependency of respiratory metabolism and phenazine-associated physiology in *Pseudomonas aeruginosa* PA14. J Bacteriol 202:e00700-19. https://doi.org/10.1128/JB.00700-19
32. Kang J, Cho Y-H, Lee Y. 2022. Pyocyanin and 1-hydroxyphenazine promote anaerobic killing of *Pseudomonas aeruginosa* via single-electron transfer with ferrous iron. Microbiol Spectr 10:e0231222. https://doi.org/10.1128/spectrum.02312-22
33. Bastos RW, Akiyama D, dos Reis TF, Colabardini AC, Luperini RS, de Castro PA, Baldini RL, Fill T, Goldman GH. 2022. Secondary metabolites produced during *Aspergillus fumigatus* and *Pseudomonas aeruginosa* biofilm formation. mBio 13:e0185022. https://doi.org/10.1128/mbio.01850-22
34. Dahlstrom KM, Newman DK. 2022. Soil bacteria protect fungi from phenazines by acting as toxin sponges. Curr Biol 32:275–288. https://doi.org/10.1016/j.cub.2021.11.002
35. Meirelles LA, Newman DK. 2022. Phenazines and toxoflavin act as interspecies modulators of resilience to diverse antibiotics. Mol Microbiol 117:1384–1404. https://doi.org/10.1111/mmi.14915
36. Schalk IJ, Perraud Q. 2023. *Pseudomonas aeruginosa* and its multiple strategies to access iron. Environ Microbiol 25:811–831. https://doi.org/10.1111/1462-2920.16328
37. Patteson JB, Putz AT, Tao L, Simke WC, Bryant LH, Britt RD, Li B. 2021. Biosynthesis of fluopsin C, a copper-containing antibiotic from *Pseudomonas aeruginosa*. Science 374:1005–1009. https://doi.org/10.1126/science.abj6749
38. Liu Y, McQuillen EA, Rana P, Gloag ES, Parsek MR, Wozniak DJ. 2024. A bacterial pigment provides cross-species protection from H_2O_2- and

Downloaded from https://journals.asm.org/journal/msystems on 06 November 2026 by 139.78.244.80.

Downloaded from https://journals.asm.org/journal/msystems on 06 November 2026 by 139.78.244.80.

neutrophil-mediated killing. Proc Natl Acad Sci USA 121:e2312334121. https://doi.org/10.1073/pnas.2312334121
39. Rossi E, La Rosa R, Bartell JA, Marvig RL, Haagensen JAJ, Sommer LM, Molin S, Johansen HK. 2021. *Pseudomonas aeruginosa* adaptation and evolution in patients with cystic fibrosis. Nat Rev Microbiol 19:331–342. https://doi.org/10.1038/s41579-020-00477-5
40. Neve RL, Giedraitis E, Akbari MS, Cohen S, Phelan VV. 2024. Secondary metabolite profiling of *Pseudomonas aeruginosa* isolates reveals rare genomic traits. mSystems 9:e0033924. https://doi.org/10.1128/msystems.00339-24
41. Nguyen AT, O'Neill MJ, Watts AM, Robson CL, Lamont IL, Wilks A, Oglesby-Sherrouse AG. 2014. Adaptation of iron homeostasis pathways by a *Pseudomonas aeruginosa* pyoverdine mutant in the cystic fibrosis lung. J Bacteriol 196:2265–2276. https://doi.org/10.1128/JB.01491-14
42. Kang D, Revtovich AV, Chen Q, Shah KN, Cannon CL, Kirienko NV. 2019. Pyoverdine-dependent virulence of *Pseudomonas aeruginosa* isolates from cystic fibrosis patients. Front Microbiol 10:2048. https://doi.org/10.3389/fmicb.2019.02048
43. Johnson JS, Spakowicz DJ, Hong B-Y, Petersen LM, Demkowicz P, Chen L, Leopold SR, Hanson BM, Agresta HO, Gerstein M, Sodergren E, Weinstock GM. 2019. Evaluation of 16S rRNA gene sequencing for species and strain-level microbiome analysis. Nat Commun 10:5029. https://doi.org/10.1038/s41467-019-13036-1
44. Hassler HB, Probert B, Moore C, Lawson E, Jackson RW, Russell BT, Richards VP. 2022. Phylogenies of the 16S rRNA gene and its hypervariable regions lack concordance with core genome phylogenies. Microbiome 10:104. https://doi.org/10.1186/s40168-022-01295-y
45. Blanchard AC, Waters VJ. 2019. Microbiology of cystic fibrosis airway disease. Semin Respir Crit Care Med 40:727–736. https://doi.org/10.1055/s-0039-1698464
46. Otto M. 2009. *Staphylococcus epidermidis* — the 'accidental' pathogen. Nat Rev Microbiol 7:555–567. https://doi.org/10.1038/nrmicro2182
47. Filkins LM, Hampton TH, Gifford AH, Gross MJ, Hogan DA, Sogin ML, Morrison HG, Paster BJ, O'Toole GA. 2012. Prevalence of streptococci and increased polymicrobial diversity associated with cystic fibrosis patient stability. J Bacteriol 194:4709–4717. https://doi.org/10.1128/JB.00566-12
48. Scott JE, O'Toole GA. 2019. The Yin and Yang of *Streptococcus* lung infections in cystic fibrosis: a model for studying polymicrobial interactions. J Bacteriol 201:1–11. https://doi.org/10.1128/JB.00115-19
49. Moran Losada P, Chouvarine P, Dorda M, Hedtfeld S, Mielke S, Schulz A, Wiehlmann L, Tümmler B. 2016. The cystic fibrosis lower airways microbial metagenome. ERJ Open Res 2:00096-2015. https://doi.org/10.1183/23120541.00096-2015
50. Pienkowska K, Pust M-M, Gessner M, Gaedcke S, Thavarasa A, Rosenboom I, Morán Losada P, Minso R, Arnold C, Hedtfeld S, Dorda M, Wiehlmann L, Mainz JG, Klockgether J, Tümmler B. 2023. The cystic fibrosis upper and lower airway metagenome. Microbiol Spectr 11:e0363322. https://doi.org/10.1128/spectrum.03633-22
51. Khanolkar RA, Clark ST, Wang PW, Hwang DM, Yau YCW, Waters VJ, Guttman DS. 2020. Ecological succession of polymicrobial communities in the cystic fibrosis airways. mSystems 5:e00809-20. https://doi.org/10.1128/mSystems.00809-20
52. Cuthbertson L, Walker AW, Oliver AE, Rogers GB, Rivett DW, Hampton TH, Ashare A, Elborn JS, De Soyza A, Carroll MP, Hoffman LR, Lanyon C, Moskowitz SM, O'Toole GA, Parkhill J, Planet PJ, Teneback CC, Tunney MM, Zuckerman JB, Bruce KD, van der Gast CJ. 2020. Lung function and microbiota diversity in cystic fibrosis. Microbiome 8:45. https://doi.org/10.1186/s40168-020-00810-3
53. Escapa IF, Chen T, Huang Y, Gajare P, Dewhirst FE, Lemon KP. 2018. New insights into human nostril microbiome from the expanded human oral microbiome database (eHOMD): a resource for the microbiome of the human aerodigestive tract. mSystems 3:e00187-18. https://doi.org/10.1128/mSystems.00187-18
54. Vogt SL, Green C, Stevens KM, Day B, Erickson DL, Woods DE, Storey DG. 2011. The stringent response is essential for *Pseudomonas aeruginosa* virulence in the rat lung agar bead and *Drosophila melanogaster* feeding models of infection. Infect Immun 79:4094–4104. https://doi.org/10.1128/IAI.00193-11
55. Schafhauser J, Lepine F, McKay G, Ahlgren HG, Khakimova M, Nguyen D. 2014. The stringent response modulates 4-hydroxy-2-alkylquinoline biosynthesis and quorum-sensing hierarchy in *Pseudomonas aeruginosa*. J Bacteriol 196:1641–1650. https://doi.org/10.1128/JB.01086-13
56. Higgins S, Heeb S, Rampioni G, Fletcher MP, Williams P, Cámara M. 2018. Differential regulation of the phenazine biosynthetic operons by quorum sensing in *Pseudomonas aeruginosa* PAO1-N. Front Cell Infect Microbiol 8:252. https://doi.org/10.3389/fcimb.2018.00252
57. Weiser R, Oakley J, Ronchetti K, Tame J-D, Hoehn S, Jurkowski TP, Mahenthiralingam E, Forton JT. 2022. The lung microbiota in children with cystic fibrosis captured by induced sputum sampling. J Cyst Fibros 21:1006–1012. https://doi.org/10.1016/j.jcf.2022.01.006
58. VanDevanter DR, LiPuma JJ, Konstan MW. 2024. Longitudinal bacterial prevalence in cystic fibrosis airways: fact and artifact. J Cyst Fibros 23:58–64. https://doi.org/10.1016/j.jcf.2023.09.011
59. Fischer AJ, Planet PJ. 2024. A birth cohort approach to understanding cystic fibrosis lung infections. J Cyst Fibros 23:8–11. https://doi.org/10.1016/j.jcf.2023.10.014
60. Zemanick ET, Wagner BD, Robertson CE, Ahrens RC, Chmiel JF, Clancy JP, Gibson RL, Harris WT, Kurland G, Laguna TA, McColley SA, McCoy K, Retsch-Bogart G, Sobush KT, Zeitlin PL, Stevens MJ, Accurso FJ, Sagel SD, Harris JK. 2017. Airway microbiota across age and disease spectrum in cystic fibrosis. Eur Respir J 50:1700832. https://doi.org/10.1183/13993003.00832-2017
61. Thomas SR. 2000. Increased sputum amino acid concentrations and auxotrophy of *Pseudomonas aeruginosa* in severe cystic fibrosis lung disease. Thorax 55:795–797. https://doi.org/10.1136/thorax.55.9.795
62. Hoffman LR, Richardson AR, Houston LS, Kulasekara HD, Martens-Habbena W, Klausen M, Burns JL, Stahl DA, Hassett DJ, Fang FC, Miller SI. 2010. Nutrient availability as a mechanism for selection of antibiotic tolerant *Pseudomonas aeruginosa* within the CF Airway. PLoS Pathog 6:e1000712. https://doi.org/10.1371/journal.ppat.1000712
63. Wilson R, Sykes DA, Watson D, Rutman A, Taylor GW, Cole PJ. 1988. Measurement of *Pseudomonas aeruginosa* phenazine pigments in sputum and assessment of their contribution to sputum sol toxicity for respiratory epithelium. Infect Immun 56:2515–2517. https://doi.org/10.1128/iai.56.9.2515-2517.1988
64. Middleton B, Rodgers HC, Cámara M, Knox AJ, Williams P, Hardman A. 2002. Direct detection of *N*-acylhomoserine lactones in cystic fibrosis sputum. FEMS Microbiol Lett 207:1–7. https://doi.org/10.1111/j.1574-6968.2002.tb11019.x
65. Quinn RA, Phelan VV, Whiteson KL, Garg N, Bailey BA, Lim YW, Conrad DJ, Dorrestein PC, Rohwer FL. 2016. Microbial, host and xenobiotic diversity in the cystic fibrosis sputum metabolome. ISME J 10:1483–1498. https://doi.org/10.1038/ismej.2015.207
66. Moebius N, Ross C, Scherlach K, Rohm B, Roth M, Hertweck C. 2012. Biosynthesis of the respiratory toxin bongkrekic acid in the pathogenic bacterium *Burkholderia gladioli*. Chem Biol 19:1164–1174. https://doi.org/10.1016/j.chembiol.2012.07.022
67. Ross C, Opel V, Scherlach K, Hertweck C. 2014. Biosynthesis of antifungal and antibacterial polyketides by *Burkholderia gladioli* in coculture with *Rhizopus microsporus*. Mycoses 57:48–55. https://doi.org/10.1111/myc.12246
68. Song L, Jenner M, Masschelein J, Jones C, Bull MJ, Harris SR, Hartkoorn RC, Vocat A, Romero-Canelon I, Coupland P, Webster G, Dunn M, Weiser R, Paisey C, Cole ST, Parkhill J, Mahenthiralingam E, Challis GL. 2017. Discovery and biosynthesis of gladiolin: a *Burkholderia gladioli* antibiotic with promising activity against *Mycobacterium tuberculosis*. J Am Chem Soc 139:7974–7981. https://doi.org/10.1021/jacs.7b03382
69. Jenul C, Sieber S, Daeppen C, Mathew A, Lardi M, Pessi G, Hoepfner D, Neuburger M, Linden A, Gademann K, Eberl L. 2018. Biosynthesis of fragin is controlled by a novel quorum sensing signal. Nat Commun 9:1297. https://doi.org/10.1038/s41467-018-03690-2
70. Dashti Y, Nakou IT, Mullins AJ, Webster G, Jian X, Mahenthiralingam E, Challis GL. 2020. Discovery and biosynthesis of *Bolagladins*: unusual lipodepsipeptides from *Burkholderia gladioli* clinical isolates. Angew Chem Int Ed 59:21553–21561. https://doi.org/10.1002/anie.202009110
71. Nakou IT, Jenner M, Dashti Y, Romero-Canelón I, Masschelein J, Mahenthiralingam E, Challis GL. 2020. Genomics-driven discovery of a novel glutarimide antibiotic from *Burkholderia gladioli* reveals an unusual polyketide synthase chain release mechanism. Angew Chem Int Ed Engl 59:23145–23153. https://doi.org/10.1002/anie.202009007
72. McAvoy AC, Jaiyesimi O, Threatt PH, Seladi T, Goldberg JB, da Silva RR, Garg N. 2020. Differences in cystic fibrosis-associated *Burkholderia* spp. bacteria metabolomes after exposure to the antibiotic trimethoprim. ACS Infect Dis 6:1154–1168. https://doi.org/10.1021/acsinfecdis.9b00513

Downloaded from https://journals.asm.org/journal/msystems on 06 November 2026 by 139.78.244.80.

73. Jones C, Webster G, Mullins AJ, Jenner M, Bull MJ, Dashti Y, Spilker T, Parkhill J, Connor TR, LiPuma JJ, Challis GL, Mahenthiralingam E. 2021. Kill and cure: genomic phylogeny and bioactivity of *Burkholderia gladioli* bacteria capable of pathogenic and beneficial lifestyles. Microb Genom 7:mgen000515. https://doi.org/10.1099/mgen.0.000515
74. Jaiyesimi OA, McAvoy AC, Fogg DN, Garg N. 2021. Metabolomic profiling of *Burkholderia cenocepacia* in synthetic cystic fibrosis sputum medium reveals nutrient environment-specific production of virulence factors. Sci Rep 11:21419. https://doi.org/10.1038/s41598-021-00421-4
75. McAvoy AC, Threatt PH, Kapcia J, Garg N. 2023. Discovery of homogentisic acid as a precursor in trimethoprim metabolism and natural product biosynthesis. ACS Chem Biol 18:711–723. https://doi.org/10.1021/acschembio.2c00529
76. Marvig RL, Sommer LM, Molin S, Johansen HK. 2015. Convergent evolution and adaptation of *Pseudomonas aeruginosa* within patients with cystic fibrosis. Nat Genet 47:57–64. https://doi.org/10.1038/ng.3148
77. Lozano C, Azcona-Gutiérrez JM, Van Bambeke F, Sáenz Y. 2018. Great phenotypic and genetic variation among successive chronic *Pseudomonas aeruginosa* from a cystic fibrosis patient. PLoS One 13:e0204167. https://doi.org/10.1371/journal.pone.0204167
78. Hissen AHT, Chow JMT, Pinto LJ, Moore MM. 2004. Survival of *Aspergillus fumigatus* in serum involves removal of iron from transferrin: the role of siderophores. Infect Immun 72:1402–1408. https://doi.org/10.1128/IAI.72.3.1402-1408.2004
79. Bertrand S, Larcher G, Landreau A, Richomme P, Duval O, Bouchara J-P. 2009. Hydroxamate siderophores of *Scedosporium apiospermum*. Biometals 22:1019–1029. https://doi.org/10.1007/s10534-009-9253-0
80. Bignell E, Cairns TC, Throckmorton K, Nierman WC, Keller NP. 2016. Secondary metabolite arsenal of an opportunistic pathogenic fungus. Philos Trans R Soc Lond B Biol Sci 371:20160023. https://doi.org/10.1098/rstb.2016.0023
81. Staerck C, Landreau A, Herbette G, Roullier C, Bertrand S, Siegler B, Larcher G, Bouchara J-P, Fleury MJJ. 2017. The secreted polyketide boydone A is responsible for the anti-*Staphylococcus aureus* activity of *Scedosporium boydii*. FEMS Microbiol Lett 364. https://doi.org/10.1093/femsle/fnx223
82. Le Govic Y, Havlíček V, Capilla J, Luptáková D, Dumas D, Papon N, Le Gal S, Bouchara J-P, Vandeputte P. 2020. Synthesis of the hydroxamate siderophore Nα-methylcoprogen B in *Scedosporium apiospermum* is mediated by sidD ortholog and is required for virulence. Front Cell Infect Microbiol 10:587909. https://doi.org/10.3389/fcimb.2020.587909
83. Aguiar M, Orasch T, Shadkchan Y, Caballero P, Pfister J, Sastré-Velásquez LE, Gsaller F, Decristoforo C, Osherov N, Haas H. 2022. Uptake of the siderophore *Triacetylfusarinine* C, but not fusarinine C, is crucial for virulence of *Aspergillus fumigatus*. mBio 13:e0219222. https://doi.org/10.1128/mbio.02192-22
84. Armbruster CR, Coenye T, Touqui L, Bomberger JM. 2020. Interplay between host-microbe and microbe-microbe interactions in cystic fibrosis. J Cyst Fibros 19:S47–S53. https://doi.org/10.1016/j.jcf.2019.10.015
85. Kramer R, Sauer-Heilborn A, Welte T, Jauregui R, Brettar I, Guzman CA, Höfle MG. 2015. High individuality of respiratory bacterial communities in a large cohort of adult cystic fibrosis patients under continuous antibiotic treatment. PLoS One 10:e0117436. https://doi.org/10.1371/journal.pone.0117436
86. Hogan DA, Willger SD, Dolben EL, Hampton TH, Stanton BA, Morrison HG, Sogin ML, Czum J, Ashare A. 2016. Analysis of lung microbiota in bronchoalveolar lavage, protected brush and sputum samples from subjects with mild-to-moderate cystic fibrosis lung disease. PLoS One 11:e0149998. https://doi.org/10.1371/journal.pone.0149998
87. Pittman JE, Wylie KM, Akers K, Storch GA, Hatch J, Quante J, Frayman KB, Clarke N, Davis M, Stick SM, Hall GL, Montgomery G, Ranganathan S, Davis SD, Ferkol TW, Australian Respiratory Early Surveillance Team for Cystic Fibrosis. 2017. Association of antibiotics, airway microbiome, and inflammation in infants with cystic fibrosis. Ann Am Thorac Soc 14:1548–1555. https://doi.org/10.1513/AnnalsATS.201702-121OC
88. Grahl N, Dolben EL, Filkins LM, Crocker AW, Willger SD, Morrison HG, Sogin ML, Ashare A, Gifford AH, Jacobs NJ, Schwartzman JD, Hogan DA. 2018. Profiling of bacterial and fungal microbial communities in cystic fibrosis sputum using RNA. mSphere 3:e00292-18. https://doi.org/10.1128/mSphere.00292-18
89. Kramná L, Dřevínek P, Lin J, Kulich M, Cinek O. 2018. Changes in the lung bacteriome in relation to antipseudomonal therapy in children with cystic fibrosis. Folia Microbiol 63:237–248. https://doi.org/10.1007/s12223-017-0562-3
90. Peleg AY, Choo JM, Langan KM, Edgeworth D, Keating D, Wilson J, Rogers GB, Kotsimbos T. 2018. Antibiotic exposure and interpersonal variance mask the effect of ivacaftor on respiratory microbiota composition. J Cyst Fibros 17:50–56. https://doi.org/10.1016/j.jcf.2017.08.002
91. Terranova L, Oriano M, Teri A, Ruggiero L, Tafuro C, Marchisio P, Gramegna A, Contarini M, Franceschi E, Sottotetti S, Cariani L, Bevivino A, Chalmers JD, Aliberti S, Blasi F. 2018. How to process sputum samples and extract bacterial DNA for microbiota analysis. Int J Mol Sci 19:3256. https://doi.org/10.3390/ijms19103256
92. Jorth P, Ehsan Z, Rezayat A, Caldwell E, Pope C, Brewington JJ, Goss CH, Benscoter D, Clancy JP, Singh PK. 2019. Direct lung sampling indicates that established pathogens dominate early infections in children with cystic fibrosis. Cell Rep 27:1190–1204. https://doi.org/10.1016/j.celrep.2019.03.086
93. Keravec M, Mounier J, Guilloux C-A, Fangous M-S, Mondot S, Vallet S, Gouriou S, Le Berre R, Rault G, Férec C, Barbier G, Lepage P, Héry-Arnaud G. 2019. *Porphyromonas*, a potential predictive biomarker of *Pseudomonas aeruginosa* pulmonary infection in cystic fibrosis. BMJ Open Respir Res 6:e000374. https://doi.org/10.1136/bmjresp-2018-000374
94. Quinn RA, Adem S, Mills RH, Comstock W, DeRight Goldasich L, Humphrey G, Aksenov AA, Melnik AV, da Silva R, Ackermann G, Bandeira N, Gonzalez DJ, Conrad D, O'Donoghue AJ, Knight R, Dorrestein PC. 2019. Neutrophilic proteolysis in the cystic fibrosis lung correlates with a pathogenic microbiome. Microbiome 7:23. https://doi.org/10.1186/s40168-019-0636-3
95. de Almeida OGG, Capizzani CP da C, Tonani L, Grizante Barião PH, da Cunha AF, De Martinis ECP, Torres LAGMM, von Zeska Kress MR. 2020. The lung microbiome of three young Brazilian patients with cystic fibrosis colonized by fungi. Front Cell Infect Microbiol 10:598938. https://doi.org/10.3389/fcimb.2020.598938
96. Flynn S, Reen FJ, Caparrós-Martín JA, Woods DF, Peplies J, Ranganathan SC, Stick SM, O'Gara F. 2020. Bile acid signal molecules associate temporally with respiratory inflammation and microbiome signatures in clinically stable cystic fibrosis patients. Microorganisms 8:1741. https://doi.org/10.3390/microorganisms8111741
97. Lu J, Carmody LA, Opron K, Simon RH, Kalikin LM, Caverly LJ, LiPuma JJ. 2020. Parallel analysis of cystic fibrosis sputum and saliva reveals overlapping communities and an opportunity for sample decontamination. mSystems 5:e00296-20. https://doi.org/10.1128/mSystems.00296-20
98. Maestrali FGO, Pilan RRM, Athanazio R, Sparvoli LG, Cortez RV, Taddei CR, Voegels RL. 2020. Cystic fibrosis microbiome: analysis of nasal middle meatus and sputum in different lung disease stages. RHINOL 3:225–237. https://doi.org/10.4193/RHINOL/20.040
99. Soret P, Vandenborght L-E, Francis F, Coron N, Enaud R, Avalos M, Schaeverbeke T, Berger P, Fayon M, Thiebaut R, Delhaes L, Mucofong Investigation Group. 2020. Respiratory mycobiome and suggestion of inter-kingdom network during acute pulmonary exacerbation in cystic fibrosis. Sci Rep 10:3589. https://doi.org/10.1038/s41598-020-60015-4
100. Valentini TD, Lucas SK, Binder KA, Cameron LC, Motl JA, Dunitz JM, Hunter RC. 2020. Bioorthogonal non-canonical amino acid tagging reveals translationally active subpopulations of the cystic fibrosis lung microbiota. Nat Commun 11:2287. https://doi.org/10.1038/s41467-020-16163-2
101. Whelan FJ, Waddell B, Syed SA, Shekarriz S, Rabin HR, Parkins MD, Surette MG. 2020. Culture-enriched metagenomic sequencing enables in-depth profiling of the cystic fibrosis lung microbiota. Nat Microbiol 5:379–390. https://doi.org/10.1038/s41564-019-0643-y
102. Khalaf RT, Furuta GT, Wagner BD, Robertson CE, Andrews R, Stevens MJ, Fillon SA, Zemanick ET, Harris JK. 2021. Influence of acid blockade on the aerodigestive tract microbiome in children with cystic fibrosis. J Pediatr Gastroenterol Nutr 72:520–527. https://doi.org/10.1097/MPG.0000000000003010
103. Linnane B, Walsh AM, Walsh CJ, Crispie F, O'Sullivan O, Cotter PD, McDermott M, Renwick J, McNally P. 2021. The lung microbiome in young children with cystic fibrosis: a prospective cohort study. Microorganisms 9:492. https://doi.org/10.3390/microorganisms9030492
104. Neerincx AH, Whiteson K, Phan JL, Brinkman P, Abdel-Aziz MI, Weersink EJM, Altenburg J, Majoor CJ, Maitland-van der Zee AH, Bos LDJ. 2021.

Downloaded from https://journals.asm.org/journal/msystems on 06 November 2026 by 139.78.244.80.

Lumacaftor/ivacaftor changes the lung microbiome and metabolome in cystic fibrosis patients. ERJ Open Res 7:00731–02020. https://doi.org/10.1183/23120541.00731-2020
105. Frey DL, Bridson C, Dittrich S, Graeber SY, Stahl M, Wege S, Herth F, Sommerburg O, Schultz C, Dalpke A, Mall MA, Boutin S. 2022. Changes in microbiome dominance are associated with declining lung function and fluctuating inflammation in people with cystic fibrosis. Front Microbiol 13:885822. https://doi.org/10.3389/fmicb.2022.885822
106. Widder S, Zhao J, Carmody LA, Zhang Q, Kalikin LM, Schloss PD, LiPuma JJ. 2022. Association of bacterial community types, functional microbial processes and lung disease in cystic fibrosis airways. ISME J 16:905–914. https://doi.org/10.1038/s41396-021-01129-z
107. Caparrós-Martín JA, Saladie M, Agudelo-Romero SP, Reen FJ, Ware RS, Sly PD, Stick SM, O'Gara F, COMBAT study group. 2023. Detection of bile acids in bronchoalveolar lavage fluid defines the inflammatory and microbial landscape of the lower airways in infants with cystic fibrosis. Microbiome 11:132. https://doi.org/10.1186/s40168-023-01543-9
108. Knoll RL, Jarquín-Díaz VH, Klopp J, Kemper A, Hilbert K, Hillen B, Pfirrmann D, Simon P, Bähner V, Nitsche O, Gehring S, Markó L, Forslund SK, Poplawska K. 2023. Resilience and stability of the CF-intestinal and respiratory microbiome during nutritional and exercise intervention. BMC Microbiol 23:44. https://doi.org/10.1186/s12866-023-02788-y
109. Martin C, Guzior DV, Gonzalez CT, Okros M, Mielke J, Padillo L, Querido G, Gil M, Thomas R, McClelland M, Conrad D, Widder S, Quinn RA. 2023. Longitudinal microbial and molecular dynamics in the cystic fibrosis lung after Elexacaftor–Tezacaftor–Ivacaftor therapy. Respir Res 24:317. https://doi.org/10.1186/s12931-023-02630-z
110. Nichols DP, Morgan SJ, Skalland M, Vo AT, Van Dalfsen JM, Singh SB, Ni W, Hoffman LR, McGeer K, Heltshe SL, Clancy JP, Rowe SM, Jorth P, Singh PK, PROMISE-Micro Study Group. 2023. Pharmacologic improvement of CFTR function rapidly decreases sputum pathogen density, but lung infections generally persist. J Clin Invest 133:e167957. https://doi.org/10.1172/JCI167957
111. Armbruster CR, Hilliam YK, Zemke AC, Atteih S, Marshall CW, Moore J, Koirala J, Krainz L, Gaston JR, Lee SE, Cooper VS, Bomberger JM. 2024. Persistence and evolution of *Pseudomonas aeruginosa* following initiation of highly effective modulator therapy in cystic fibrosis. mBio 15:e0051924. https://doi.org/10.1128/mbio.00519-24
112. Frayman KB, Macowan M, Caparros-Martin J, Ranganathan SC, Marsland BJ, SYNERGY CF. 2024. The longitudinal microbial and metabolic landscape of infant cystic fibrosis: the gut-lung axis. Eur Respir J 63:2302290. https://doi.org/10.1183/13993003.02290-2023
113. Nassirnia S, Scherz V, Greub G, Caruana G, Taffé P, Jaton K, Papis S, Posfay-Barbe KM, Mornand A, Rochat-Guignard I, Bertelli C, Asner SA. 2024. Concordance between upper and lower airway microbiota in children with Cystic Fibrosis. medRxiv. https://doi.org/10.1101/2024.11.30.24318234
114. Widder S, Carmody LA, Opron K, Kalikin LM, Caverly LJ, LiPuma JJ. 2024. Microbial community organization designates distinct pulmonary exacerbation types and predicts treatment outcome in cystic fibrosis. Nat Commun 15:4889. https://doi.org/10.1038/s41467-024-49150-y
115. Angebault C, Vandenborght L, Bassinet L, Wizla N, Ferroni A, Dessein R, Remus N, Thumerelle C, Fauchet N, Epaud R, Delhaes L, Botterel F. 2025. Airway mycobiota—microbiota during pulmonary exacerbation of cystic fibrosis patients: a culture and targeted sequencing study. Mycoses 68:e70024. https://doi.org/10.1111/myc.70024
116. González CT, Martin C, Crane M, Gutierrez K, Thomas J, Remisoski L, Okros M, Fu Y, Guzior DV, Finkhouse D, Bridges C, Mielke J, Querido G, Padillo L, Girgis R, McClelland M, Conrad D, Li X, Quinn RA. 2026. Microenvironmental effects of a non-antibiotic therapy for a chronic polymicrobial infection alter microbial physiology, competition, and virulence. ISME J 20:wraf125. https://doi.org/10.1093/ismejo/wraf125
117. Hardman M, Higgi S, Hanson L, Schutz K, Wargo MJ, Teneback CC, Daniels TWV, van der Gast C, Rivett DW. 2025. Nontuberculous mycobacteria remodel lung microbiota in cystic fibrosis-associated respiratory infections. Microbiol Spectr 13:e0038225. https://doi.org/10.1128/spectrum.00382-25
118. Hilliam Y, Armbruster CR, Atteih SE, Rapsinski GJ, Moore J, Koirala J, Krainz L, Gaston J, Williams J, Cooper VS, Lee SE, Bomberger JM. 2025. Respiratory viral infection is associated with increased *Pseudomonas* abundance in cystic fibrosis airways. bioRxiv. https://doi.org/10.1101/2025.07.08.663034
119. Knoll RL, Brauny MM, Robert E, Cloos L, Waser L, Hilbert K, Ulmer N, Hillen B, Birkner T, Bartolomaeus TUP, Nitsche O, Jarquín-Díaz VH, Lynch S, Gehring S, Maier L, Poplawska K, Forslund-Startceva SK. 2025. CFTR modulator therapy drives microbiome restructuring through improved host physiology in cystic fibrosis: the IMMProveCF phase IV trial. Nat Commun 16:10111. https://doi.org/10.1038/s41467-025-64218-z
120. Whiteside SA, McGinniss JE, Deek RA, Merenstein C, Britton N, Simon-Soro A, Oyster M, Kalman L, Brown MC, Graham-Wooten J, McDyer JF, Shah P, D'Alessio F, Cantu E, Clausen ES, Li H, Diamond JM, Bushman FD, Christie JD, Collman RG. 2026. Lung transplant for CF: Low lung bacterial burden and immune mediators in year one associate with CLAD development. J Cyst Fibros 25:52–62. https://doi.org/10.1016/j.jcf.2025.10.002
121. Chen S, Zhou Y, Chen Y, Gu J. 2018. Fastp: an ultra-fast all-in-one FASTQ preprocessor. Bioinformatics 34:i884–i890. https://doi.org/10.1093/bioinformatics/bty560
122. Schloss PD, Westcott SL, Ryabin T, Hall JR, Hartmann M, Hollister EB, Lesniewski RA, Oakley BB, Parks DH, Robinson CJ, Sahl JW, Stres B, Thallinger GG, Van Horn DJ, Weber CF. 2009. Introducing mothur: open-source, platform-independent, community-supported software for describing and comparing microbial communities. Appl Environ Microbiol 75:7537–7541. https://doi.org/10.1128/AEM.01541-09
123. Oksanen J, Blanchet FG, Friendly M, Kindt R, Legendre P, McGlinn D, Minchin PR, O'Hara RB, Simpson GL, Solymos P, Stevens MHH, Szoecs E, Wagner H. 2019. vegan: community ecology package.
124. Szczesniak R, Heltshe SL, Stanojevic S, Mayer-Hamblett N. 2017. Use of FEV_1 in cystic fibrosis epidemiologic studies and clinical trials: a statistical perspective for the clinical researcher. J Cyst Fibros 16:318–326. https://doi.org/10.1016/j.jcf.2017.01.002
125. Schindelin J, Rueden CT, Hiner MC, Eliceiri KW. 2015. The ImageJ ecosystem: an open platform for biomedical image analysis. Molecular Reproduction Devel 82:518–529. https://doi.org/10.1002/mrd.22489
126. Tautenhahn R, Patti GJ, Rinehart D, Siuzdak G. 2012. XCMS online: a web-based platform to process untargeted metabolomic data. Anal Chem 84:5035–5039. https://doi.org/10.1021/ac300698c
127. Suzuki R, Shimodaira H. 2006. Pvclust: an R package for assessing the uncertainty in hierarchical clustering. Bioinformatics 22:1540–1542. https://doi.org/10.1093/bioinformatics/btl117
128. Dissanayake E, Brockman-Schneider RA, Stubbendieck RM, Helling BA, Zhang Z, Bochkov YA, Kirkham C, Murphy TF, Ober C, Currie CR, Gern JE. 2023. Rhinovirus increases *Moraxella catarrhalis* adhesion to the respiratory epithelium. Front Cell Infect Microbiol 12:1060748. https://doi.org/10.3389/fcimb.2022.1060748
129. Wick RR, Howden BP, Stinear TP. 2025. Autocycler: long-read consensus assembly for bacterial genomes. Bioinformatics 41:btaf474. https://doi.org/10.1093/bioinformatics/btaf474
130. Kolmogorov M, Yuan J, Lin Y, Pevzner PA. 2019. Assembly of long, error-prone reads using repeat graphs. Nat Biotechnol 37:540–546. https://doi.org/10.1038/s41587-019-0072-8
131. Cheng H, Concepcion GT, Feng X, Zhang H, Li H. 2021. Haplotype-resolved *de novo* assembly using phased assembly graphs with hifiasm. Nat Methods 18:170–175. https://doi.org/10.1038/s41592-020-01056-5
132. Jain C, Rodriguez-R LM, Phillippy AM, Konstantinidis KT, Aluru S. 2018. High throughput ANI analysis of 90K prokaryotic genomes reveals clear species boundaries. Nat Commun 9:5114. https://doi.org/10.1038/s41467-018-07641-9
133. Schwengers O, Jelonek L, Dieckmann MA, Beyvers S, Blom J, Goesmann A. 2021. Bakta: rapid and standardized annotation of bacterial genomes via alignment-free sequence identification. Microb Genom 7:000685. https://doi.org/10.1099/mgen.0.000685
134. Blin K, Shaw S, Vader L, Szenei J, Reitz ZL, Augustijn HE, Cediel-Becerra JDD, de Crécy-Lagard V, Koetsier RA, Williams SE, et al. 2025. antiSMASH 8.0: extended gene cluster detection capabilities and analyses of chemistry, enzymology, and regulation. Nucleic Acids Res 53:W32–W38. https://doi.org/10.1093/nar/gkaf334
135. Wickham H. 2016. ggplot2: elegant graphics for data analysis. Springer-Verlag New York. http://ggplot2.org.